Agricultural and Forest Meteorology 353 (2024) 110037

Contents lists available at ScienceDirect

Agricultural and Forest Meteorology

journal homepage: www.elsevier.com/locate/agrformet

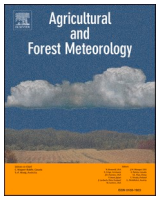

Contrasting carbon cycle responses to dry (2015 El Niño) and wet (2008 La Niña) extreme events at an Amazon tropical forest

Natalia Restrepo-Coupe [a,b,*], Kleber Silva Campos [c], Luciana F. Alves [d], Marcos Longo [e], Kenia T. Wiedemann [f], Raimundo Cosme de Oliveira Jr. [g], Luiz E.O.C. Aragao [h], Bradley O. Christoffersen [i], Plinio B. Camargo [j], Adelaine M.e S. Figueira [k], Maurício Lamano Ferreira [l], Rafael S. Oliveira [m], Deliane Penha [n], Neill Prohaska [a], Alessandro C. da Araujo [o,p], Bruce C. Daube [f], Steven C. Wofsy [f], Scott R. Saleska [a]

[a] Department of Ecology and Evolutionary Biology, University of Arizona, Tucson, AZ, United States
[b] Cupoazu LLC, Etobicoke, ON, Canada
[c] Department of Environmental Physics, Federal University of Western Pará (UFOPA), Santarém, Pará, Brazil
[d] Institute of the Environment and Sustainability, University of California – Los Angeles (UCLA), Los Angeles, CA, United States
[e] Climate and Ecosystem Sciences Division, Lawrence Berkeley National Laboratory, Berkeley, CA United States
[f] Department of Earth and Planetary Sciences, Harvard University, Massachusetts, MA, United States
[g] Brazilian Agricultural Research Corporation (Embrapa) NAPT Medio Amazonas, Santarém, Pará, Brazil
[h] National Institute for Space Research (INPE), São Paulo, São Paulo, Brazil
[i] School of Integrative Biological and Chemical Sciences, University of Texas Rio Grande Valley, Edinburg, TX United States
[j] Centro de Energia Nuclear na Agricultura, Universidade de São Paulo, Piracicaba, São Paulo, Brazil
[k] Postgraduate Program in Natural Resources, Federal University of Western Pará (UFOPA), Santarém, Pará, Brazil
[l] Department of Basic and Environmental Sciences, University of São Paulo (EEL/USP), Lorena, São Paulo, Brazil
[m] Department of Plant Biology, Universidade Estadual de Campinas (UNICAMP), Campinas, São Paulo, Brazil
[n] Postgraduate Program in Biodiversity, Federal University of Western Pará (UFOPA), Santarém, Pará, Brazil
[o] Brazilian Agricultural Research Corporation (Embrapa) Amazônia Oriental, Belém, Pará, Brazil
[p] Instituto Nacional de Pesquisas da Amazônia (INPA), Manaus, Amazonas, Brazil

ARTICLE INFO

Keywords:
Eddy covariance
Carbon
Water and energy flux seasonality
Amazonia
Tropical forests
Ecosystem-climate interactions
ENSO

ABSTRACT

Land surface models diverge in their predictions of the Amazon forest's response to climate change-induced droughts, with some showing a catastrophic collapse of forests, while others simulating resilience. Therefore, observations of tropical ecosystem responses to real-world droughts and other extreme events are needed. We report long-term seasonal dynamics of photosynthesis, respiration, net carbon exchange, phenology, and tree demography and characterize the effect of dry and wet events on ecosystem form and function at the Tapajós National Forest, Brazil, using over two decades of eddy covariance observations that include the 2015–2016 El Niño drought and La Niña 2008–2009 wet periods. We found strong forest responses to both ENSO events: La Niña saw forest net carbon loss from reduced photosynthesis (due to lower incoming radiation from increased cloudiness) even as ecosystem respiration (R_{eco}) was maintained at mean seasonal levels. El Niño induced the opposite short-term effect, net carbon gains, despite significant reductions in photosynthesis (from a drought-induced halving of canopy conductance to CO_2 and significant losses of leaf area), because drought suppression of R_{eco} losses was even greater. However, long-term responses to the two climate perturbations were very different: **transient** during La Niña –the forest returned to its "normal" state as soon as the climate did, and **long-lasting** during El Niño –leaf area loss and associated declines in photosynthetic capacity (*Pc*) and canopy conductance were exacerbated and extended by feedbacks from higher temperatures and atmospheric evaporative demand and persisted for ~3+ years after normal rainfall resumed. These findings indicate that these forests are more vulnerable to drought than to excess rain, because drought drives significant changes in forest structure (e.g., leaf-abscission and mortality) and ecosystem function (e.g. reduced stomatal conductance). As

* Corresponding author.
E-mail address: nataliacoupe@gmail.com (N. Restrepo-Coupe).

https://doi.org/10.1016/j.agrformet.2024.110037
Received 19 April 2023; Received in revised form 19 March 2024; Accepted 29 April 2024
Available online 21 May 2024

future Amazonian climate change increases frequencies of hydrological extremes, these mechanisms will determine the long-term fate of tropical forests.

1. Introduction

Tropical ecosystems are important biodiversity and biomass reservoirs, the Amazon forest being the largest contiguous tropical forest, significantly contributing to current global water, energy, carbon and other biogeochemical fluxes. Determining this ecosystem's response to climate change is important, as the frequency of extreme events (e.g., drought, heat waves, and wet periods) is increasing (IPCC, 2013; Malhi et al., 2009) and it is predicted to have a direct impact on the land-atmosphere exchange, and forest biomass, structure and demography (Barichivich et al., 2018; Davidson et al., 2012; Duffy et al., 2015; Gloor et al., 2013; Longo et al., 2018; Marengo and Espinoza, 2016; Masson-Delmotte et al., 2018; Nepstad et al., 2002; Nobre et al., 2016). For example, the study of tropical ecosystem response to wet extremes (generally characterized by a reduction in incoming radiation) has been neglected and may be key in determining forest composition (Esteban et al., 2021). Moreover, significant debate surrounds even the present-day effect of drought and seasonal water stress on tropical forests based on two arguments: (1) Water stress limits photosynthesis through hydraulic constraints, thus decreasing tree performance and increasing mortality during drought (Betts et al., 2004; Castanho et al., 2016; Cox et al., 2004; Phillips et al., 2009; Zhang et al., 2015), and (2) light availability limits forest photosynthesis and growth, leading to increases in photosynthesis during dry seasons and interannual droughts when cloud cover decreases (Bonal et al., 2016; Huete et al., 2006; Hutyra et al., 2007; Saleska et al., 2007). Furthermore, land surface models that link wet-events and drought-related variations in precipitation, atmospheric moisture and radiation to changes in tropical forest carbon-uptake; show high uncertainty on both the sign and the magnitude of the exchange (Ahlström et al., 2012; Allen et al., 2010; Sitch et al., 2008). New observations are needed to quantify relationships between environmental drivers and carbon-cycle components of photosynthesis, respiration, and allocation to growth of leaves and wood, and how these relations change throughout wet episodes, drought, and drought recovery periods.

Across Amazonia, the 2015–2016 El Niño drought brought lower river levels, drier soils, significantly higher temperatures, and increased atmospheric evaporative demand (Jiménez-Muñoz et al., 2016) exacerbating an existing drying and warming trend (Ritchie et al., 2022; Wainwright et al., 2022). Remote sensing products identified important biomass losses (Yang et al., 2022), structural and/or compositional changes (Amigo, 2020; Brando et al., 2020; Esquivel-Muelbert et al., 2019) and reduced photosynthetic activity (Jiménez-Muñoz et al., 2016), particularly in the northeast region of Amazonia. The drought impacts resulted in significant productivity reductions of 10–15 % in the eastern forests compared to 2–5 % in western ecosystems (2–5 %) (Koren et al., 2018). For instance, the western forests of Manaus became a significant source of CO_2 emissions (Botía et al., 2022). Moreover, higher vapor pressure deficit (*VPD*) and decreasing soil moisture reduced leaf production (Barro Colorado, Panama) (Detto et al., 2018), increased litter fall (Tapajós National Forest) (Oliveira de Morais et al., 2021) and limited stomatal conductivity (Panama and Tapajós) (Detto and Pacala, 2022; Restrepo-Coupe et al., 2023), the result of vegetation balancing the needs between CO_2 uptake and H_2O losses. Nonetheless, the impacts of the El Niño droughts did not always result in carbon losses. For example, at a tropical forest site in French Guiana, El Niño 2015–2016 drought conditions led to substantially lower ecosystem respiration and moderate reductions in photosynthesis, resulting in higher carbon uptake (Bonal et al., 2016). In Panama, higher solar radiation helped maintain photosynthetic activity (Bonal et al., 2016), and stimulated seed production (Detto et al., 2018). In contrast, forest inventories at intact tropical forests showed, on average, no significant biomass gain or loss after drought (Bennett et al., 2023). Differences in species composition and/or climate may explain the differences in mortality, leaf production/abscission, and vegetation response across sites. However, one clear challenge is the limited analyses of integrated micrometeorological and biometric measurements across the basin, which hampers our ability to directly link vegetation dynamics with ecosystem fluxes and physiological controls to more clearly identify mechanisms of response and forecast the short and long-term consequences of drought/wet events on tropical forest ecosystems.

The Tapajós National Forest K67 (BR-Sa1) site is one of the few long-term tropical forest eddy covariance towers with over 12 years of measurements of biometry, meteorology and carbon, water, and energy fluxes (2001–2005, 2008–2011, 2015–2020). The forest is located near the confluence of the Amazon and Tapajós rivers, close to Santarém, in the central eastern Amazon basin (Fig. S1). Observations include two exceptionally strong El Niño-Southern Oscillation (ENSO) events, the 2008–2009 La Niña, when the wet season was wetter and incoming solar radiation was lower than the seasonal average, and the 2015–2016 El Niño, one of the strongest droughts on record (Kim et al., 2011; Marengo and Espinoza, 2016) (Fig. S1). Across Amazonia the Santarém region shows one of the most significant correlations between rainfall and ENSO cycles of drought and flood (Fig. S1). Consequently, our measurements provide a unique opportunity to detect forest responses to meteorological drivers and seasonal and long-term phenology, carbon fluxes, and canopy structure characteristics.

Our work aims (1) to quantify changes in carbon flux during drought and wet events to elucidate how (i) meteorological conditions, (ii) seasonal phenology (represented by the dynamics of ecosystem photosynthetic capacity and leaf area index), and (iii) short-term physiological responses (represented by ecosystem-level stomatal conductance) drive higher CO_2 uptake or efflux at a tropical forest site; (2) to determine which of the carbon exchange components — photosynthesis measured as the gross ecosystem productivity (*GEP*) or ecosystem respiration (R_{eco}) — dominate the observed net ecosystem exchange ($NEE = GEP+R_{eco}$), and (3) to examine the longer-term effect (1 to 3 years) of drought/wet periods on meteorology, canopy structure, phenology and carbon flux. Our analysis guides improvements in understanding tropical forest form and function, the long term consequences of ENSO events, and how tropical rainforests may show resilience and recovery.

2. Methods

2.1. Site description

To understand seasonal tropical forest-atmosphere exchange we measured carbon, water and energy fluxes using the eddy covariance (EC) method at a 64 m tower located in the equatorial Amazon (2.857 S, 54.959 W) near the town of Santarém, Pará, Brazil. The EC system and biometry transects were established in 2000 as part of the ecological component of the Brazilian-led Large Scale Biosphere-Atmosphere experiment in Amazonia (LBA). The forest canopy has an average height of 40 m and a total of 249 species (133 sp ha^{-1}) have been identified at the site (Vieira et al., 2004). The dominant species at the site are *Erisma uncinatum, Manilkara elata*, and *Chamaecrista xinguensis*, accounting for 12.8 %, 7.8 % and 6.6 % of the total basal area, respectively (Alves et al. in preparation). The forest's soils have low organic carbon content and cation exchange capacity and they are predominantly nutrient-poor clay oxisols and sandy ultisols (Silver et al., 2000). The site ecology has been previously described in Saleska et al. (2003), Rice et al. (2004), Pyle et al. (2008), and Hutyra et al. (2007).

2.2. Eddy covariance measurements

Hourly carbon (*Fc*; $\mu mol_{CO2}\ m^{-2}\ s^{-1}$), water ($F_{H2O}$; mmol $m^{-2}\ s^{-1}$), sensible heat (*H*; W m^{-2}) and momentum (τ; kg $m^{-2}\ s^{-2}$) fluxes were calculated as proportional to the mean covariance between fluctuations of vertical velocity measured by a sonic anemometer and the corresponding scalar – CO_2, H_2O vapor, temperature and horizontal wind velocity, respectively (Oke, 2015). A close path infrared gas analyzer (IRGA) measured CO_2 and H_2O. The IRGA was calibrated (zero or no H_2O or CO_2 flux) every four hours using N_2 dry air gas and at least every 12 hours running a sequence of air with a known low, medium and high CO_2 concentration (e.g. 330, 420 and 480 ppm). The CO_2 concentration of the calibration air was regularly modified to adjust for the increase in atmospheric CO_2. The H_2O span was determined using ancillary relative humidity (RH;%) measurements or assuming air moisture at saturation during the night time. See supplementary information (SI) Table S1 for EC and ancillary meteorological instrumentation.

Hourly turbulent fluxes were subject to quality control by removing rainy periods (e.g. raindrops blocking the anemometer path), outliers due to instrument malfunction (e.g. pump failure), when the calibration system failed (e.g. N_2 gas run-out) and measurements under low turbulence conditions using a friction velocity (u_*; m s^{-1}) threshold of 0.22 ± 0.02 m s^{-1} (see SI Section 1 and Fig. S2). Fluxes correspond to the periods: 2002 - 2005, July 2008 - December 2012 and January 2015 - July 2020 with few interruptions.

2.3. Measurement and calculation of water, carbon and energy cycle components

The net ecosystem exchange (*NEE*; μmol $m^{-2}\ s^{-1}$) was calculated as the sum of the fluxes measured at the top of the tower and the CO_2 storage flux ($NEE = Fc + S_{CO2}$) and defined as negative to represent carbon-uptake by the forest. The ecosystem respiration (R_{eco}; μmol $m^{-2}\ s^{-1}$) was calculated by a 5-day to 30-day nighttime *NEE* moving window (minimum of eight available hours). Daytime R_{eco} was assumed to be equal to nighttime R_{eco} as no linear or exponential relationship was found between nighttime *NEE* and T_{air} (Fig. S3) (Restrepo-Coupe et al., 2017). The gross ecosystem exchange (*GEE*; μmol $m^{-2}\ s^{-1}$) was estimated from the measured daytime by subtracting R_{eco} ($GEE = -NEE + R_{eco}$). Gross ecosystem productivity (*GEP*; μmol $m^{-2}\ s^{-1}$) was assumed as the negative *GEE*, where *GEP*=-*GEE* (Stoy et al., 2006). Light response curves were used to fill a few missing *GEP* values (gaps with a maximum of 40 continuous hours) (Fig. S4). Seasonal carbon flux values presented in units of gC $m^{-2}\ d^{-1}$.

To represent the capacity of the canopy to assimilate CO_2 via photosynthesis, independent of short term variation in environmental drivers, we estimated the ecosystem photosynthetic capacity (*Pc;* gC $m^{-2}\ d^{-1}$). The seasonal *Pc* was calculated as the average *GEP* for a 16-day period measured under fixed narrow meteorological conditions represented by bins of photosynthetic active radiation (*PAR;* μmol $m^{-2}\ s^{-1}$) (i.e. between the mean annual daytime *PAR* value of 836 ± 200 μmol $m^{-2}\ s^{-1}$) and daytime mean ± one standard deviation of air temperature (T_{air}; C) (27.22±2.04 °C), vapor pressure deficit (*VPD; kPa)* (1.02±0.45 kPa), and cloudiness index (*CI*) (0.44±0.14) (Restrepo-Coupe et al., 2017; Wu et al., 2016). *PAR, T_{air}* and *VPD* were measured at the top of the EC tower and the *CI* was calculated as 1 minus the ratio of observed *PAR* to the theoretical *PAR* (PAR_{theo}). Where PAR_{theo} was derived from estimates of top of the atmosphere radiation (see Section 2.7). *CI* ranges between no clouds (*CI*=0) and all radiation being diffuse (*CI*=1).

We fitted photosynthetic light response curves –rectangular hyperbola to hourly *GEP* vs. *PAR*– to 16-day morning measurements (defined 7:00 - 12:00 LT) and determined the light-saturated net photosynthetic rate (P_{nmax}; $\mu mol_{CO2}\ m^{-2}\ s^{-1}$) and quantum yield of assimilation (α_{AM}; gC MJ^{-1}), thus those values change with leaf quality (e.g. decrease as the leaf ages (Xu et al., 2019) or under stress (Gamon, 2015)) (Fig. S4). Morning observations were selected to avoid low photosynthetic rates driven by higher afternoon *VPD* and T_{air} values (associated to low stomatal conductance) and other limitations (e.g., photoinhibition, reduced Rubisco activation and photorespiration (Koyama and Takemoto, 2014)), rather than by leaf phenology. Vegetation physiological response, represented by the canopy conductance (*Gs*; mol $m^{-2}\ s^{-1}$), was calculated directly by the flux-gradient method, which avoids the assumption of energy balance closure required by the often used Penman-Monteith method (Wehr and Saleska, 2021). The derivation of *Gs* required of F_{H2O} observations (and its equivalent evapotranspiration, *ET*, in units of mm s^{-1}). We restricted F_{H2O} measurements to periods without rainfall in the previous 12-hours assuming water fluxes were dominated by transpiration (Restrepo-Coupe et al., 2023). (See Table S3 for descriptors of vegetation form and function.)

To study the effect of T_{air} and *VPD* on hourly photosynthesis we fitted second-degree linear regressions between GEP_{sat}/PAR and *VPD* for different equal sized T_{air} bins and vice versa. With a similar analysis, we attempted to separate the effect of *VPD* and plant available water (cumulative water deficit, *CWD* as a proxy of soil moisture) on photosynthetic activity. The GEP_{sat} was defined as *GEP* at *PAR* values > 1000 μmol $m^{-2}\ s^{-1}$. By calculating GEP_{sat}/PAR we aim to remove the effect of changes in the light environment on photosynthetic activity.

We investigated the role of different mechanisms influencing photosynthesis – variation in external environmental drivers, versus variation in structure and photosynthetic capacity of the canopy – during both ENSO and non-ENSO years by expanding the model proposed by Wu et al. (2017), which itself builds on a long literature of Light-use Efficiency modeling for simple and tractable representation of photosynthesis in the field, from local to global scales (Field et al., 1995; Jarvis et al., 1976; Mahadevan et al., 2008; Monteith, 1972). In the model, *GEP* is determined by (1) the intrinsic light-use efficiency of the canopy, represented by eddy flux-observed light use efficiency (LUE_{ref}; $molCO_2\ mol^{-1}$ photons) under reference environmental conditions (parameter $f_{en.ref}$) and (2) environmental conditions, most notably *PAR* as well as potentially other environmental factors:

$$GEP_{model} = LUE_{ref} \Big/ f_{en.ref} x PAR x f_{env} \quad (1)$$

where the parameter f_{env} is a dimensionless scaling factor that adjusts for effects of *CI, VPD, PAR* saturation, and T_{air}, as: :

$$f_{env} = (1 + (k_{CI} \times CI)) \times (1 - (k_{VPD} \times VPD)) \times (1 / (1 + (PAR / PAR_o))) \times \left(1 - k_{Tair} \times \left(T_{air} - T_{opt}\right)^2\right) \quad (2)$$

where Wu et al. (2017) found that $k_{CI} = 2.056 \pm 0.065$, $f_{ENVref} = 1.225 \pm 0.021$, $k_{VPD} = 191.1e\text{-}6 \pm 3.4e\text{-}6$, and $PAR_o = 6216.4 \pm 13.8$. We observed that when applying the model to our longer dataset, that model residuals were significantly correlated with temperature, which we addressed by incorporating temperature into the model. We represented the effect of temperature with the expression ($1\text{-}k_{Tair}$ x $(T_{air}$ - $T_{opt})^2$), where T_{opt} (optimum temperature) and k_{Tair} (temperature coefficient) are parameters fitted using an iterative procedure which gave $k_{Tair} = -0.0125 \pm 0.0009$, and $T_{opt} = 26.293 \pm 0.16$ °C.

To identify the key seasonal drivers of photosynthesis during both ENSO events, the model was driven by the average monthly daily cycle for each of the environmental factors for non-ENSO years and compared GEP_{model} to the same model driven by the variables observed during the wet/drought event of 2008–2009 and 2015–2016 (e.g. only *PAR* HY2008, only *CI* HY2008, *VPD* HY2008, and LUE_{ref} HY2008) –similar to a sensitivity analysis (see SI Section 5 for model details and coefficients).

2.4. Forest dynamics

Trees with a diameter at breast height (DBH; cm) greater than 35 cm were measured, mapped and identified at four permanent 50 m x 1000 m transects that were installed in 1999 adjacent to the EC tower. Tree

stems ≥ 10 cm DBH were censored in narrower transects (10×1000 m) running down the middle of the larger sampling area (total area of 3.99 ha) (Pyle et al., 2008; Rice et al., 2004; Saleska et al., 2003). All transects (total area of 19.75 ha) were censused annually or bi-annually from 1999 to 2017 (Alves et al., 2018). Tree individual aboveground biomass (AGB; kg) was estimated from allometry (Chave et al., 2014) and carbon flows associated with annual tree growth (*Growth*; kgC m^{-2} yr^{-1}), changes in size class (including recruitment) ($\Delta_{size\ class}$; kgC m^{-2} yr^{-1}) and mortality rates (*Mortality*; kgC m^{-2} yr^{-1}) were calculated. For additional forest inventory methods see SI Section 2. Carbon allocated to leaf litter-fall ($Litter_{leaf}$, gC m^{-2} d^{-1}) and to leaf, fruits, wood and other debris ($Litter_{all}$, gC m^{-2} d^{-1}) were calculated using monthly litter traps as reported by Rice et al. (2004) and more recent litter samplings (2010 - present) some of them are here presented for the first time (Fig. S5).

Leaf area index (*LAI*; m^2 m^{-2}) was calculated using its relationship with albedo *PAR*, the ratio between incoming and reflected by the canopy *PAR*, a method modified from Doughty and Goulden (2008):

$$2PAR_{out}PAR\exp(-kLAI_{aPAR}) \quad (3)$$

where *PAR* is the incoming photosynthetic active radiation and PAR_{out} is the reflected *PAR* measured at the top of the tower, *SZA* is the solar zenith angle (*SZA*; deg), and *k is* the site-specific extinction coefficient ($k = 0.41\ \cos(SZA)^{-1}$). The LAI_{aPAR} calculations assumed constant leaf clumping and tree spatial distribution and were restricted to measurements dominated by direct radiation ($PAR>1400$ umol m^{-2} s^{-1}) and *SZA* close to zenith ($SZA<30$) to minimize the effect of light quality (changes in the ratio between diffuse and direct radiation). Refer to Table S3 for additional factors influencing *LAI* calculations, and consult SI section 6 for a comparison of LAI_{aPAR} with other *LAI* methods (Fig. S19).

Net primary productivity allocated to leaf-flush (NPP_{leaf}; gC m^{-2} d^{-1}) was estimated using a simple model where the seasonal change in photosynthetic capacity (dPc/dt) is defined by the leaf balance (leaf flush minus loss – litterfall) and the leaf-level carbon assimilation at saturating light (A_{max}; gC m^{-2} s^{-1}) scaled to ecosystem-level by the leaf mass area (*LMA*; g m^{-2}). Leaf demography was introduced on the model using the relationship between *LMA and* leaf age as described by Chavana-Bryant et al. (2016). Solving the equation resulted in $NPP_{leaf}=dPc/dt\ LMA\ A_{max}^{-1} + Litter_{leaf}$ (see Restrepo-Coupe et al. (2017) for details).

2.5. Satellite-derived precipitation and radiation and cumulative water deficit

We employed remotely sensed datasets in instances where ground-based observations were unavailable or deemed unreliable due to a significant number of gaps or sensor failures (e.g., precipitation) (Table S2). We obtained an ancillary record of precipitation and *CI* values from a near-by meteorological station located at the town of Belterra (2.63 S, 54.95 W) with observations starting in 1971 (Brazilian Institute of Meteorology, INMET). Here, we present basin-wide monthly 0.25 and 0.1 degree resolution precipitation data (1998–2019) from the Tropical Rainfall Measuring Mission (TRMM) data product (3B43-v7) (Huffman et al., 2007) and from Global Precipitation Measurement Mission (GPM-IMERG final run: 2000–2020), respectively (Huffman et al., 2014). We sampled TRMM and GPM precipitation for the K67 (BR-Sa1) site location (P_{TRMM}; mm). GPM was scaled to match TRMM values –closer to in-situ observations. Dry season was determined using a rainfall threshold value of 100 mm $month^{-1}$, as proposed by Sombroek (2001).

We obtained satellite derived incoming all-sky shortwave flux ($SW_{in\ CERES}$; W m^{-2}) and net radiation (Rn_{CERES}; W m^{-2}) at monthly 1-degree resolution from the L3B EBAF-Surface (v4) global grid from the Clouds and the Earth's Radiant Energy System (CERES) (Kato et al., 2012) and reflectance model values from the MCD43C1 v006 MODIS/Terra+Aqua BRDF/Albedo Model Parameters Daily L3 Global 0.05 Deg CMG daily product (Schaaf and Wang, 2015). We calculated the enhanced vegetation index (*EVI*) using the bidirectional reflectance distribution function (BRDF) adjusted reflectance (blue, red and green bands) for observer at nadir and solar zenith angle at 15°. The BRDF corrected *EVI* values (EVI_{SZA15}) represent canopy greenness – vegetation photosynthetic capacity independent of the influence of sun-sensor geometry on the reflectance signal (Huete et al., 2006) (see Table S2 for descriptors of satellite products).

We calculated monthly radiation and precipitation anomalies ($P_{TRMM\ anomaly}$) as the departure from the month's mean normalized by the standard deviation (Aragão et al., 2007). A simple bucket model was used to calculate the monthly cumulative water deficit (*CWD*; mm) as a function of the previous month *CWD*, current losses (*ET*; mm) and gains (P_{TRMM}). In the equation, if CWD>0, *CWD*=0. Finally, we present *CWD* as positive values (*CWD* = -*CWD*). In a previous study, Restrepo-Coupe et al. (2023) observed a statistically significant correlation between seasonal and hourly *CWD* and soil moisture values at Tapajós K67. The regression showed the strongest correlation ($R^2 = 0.9$, p-value < 0.01) when considering water content across a 0 to 10 m profile (θ; m^3 m^{-3}) and the first 5 m depth ($R^2 = 0.75$, p-value = 0.01), as opposed to the observations from deep soil moisture (7 to 10 m) ($R^2 = 0.66$, p-value < 0.01) (refer to Table S1 for soil sensor depths and SI Section 6 in Restrepo-Coupe et al. (2023) for additional information).

2.6. Hydrological year, derivation of monthly time series and other statistical analysis

Day-time hours were selected as those when the top of the atmosphere radiation (TOA; W m^{-2}) (Goudriaan, 1986) was above a 5 W m^{-2}. Variables were labeled with the subscript daytime (e.g. $GEP_{daytime}$). We calculated monthly and 16-day EC observations as the mean of the average day-time daily cycle for the period to avoid assigning less weight to hours when measurements can be scarce (e.g. late afternoon when rainfall may be common). Hydrological years were defined from the start of the dry season (July) to the end of the wet period (June) and named HY_{yyyy}, where yyyy is July's calendar year (e.g. HY2000: July2000 to June2001). We calculated the series long-time trends by applying a seasonal adjustment (removing the seasonal component) and using a stable seasonal filter (annual moving average) (Brockwell and Davis, 2002).

We present linear, second degree polynomial, rectangular hyperbola and exponential regressions when appropriate –coefficients were fitted using the least squares method. We calculated the statistical significance of all models using either the coefficient of determination (R^2), the Pearson correlation coefficient (R) and/or the p-value as a measure of probability of the null hypothesis (no correlation between variables). When both variables show some level of uncertainty and/or we wanted to minimize the effect of outliers we used Type II linear regressions. The analysis was implemented in Matlab 2019b.

3. Results

Here we contrast the seasonality of carbon fluxes, leaf phenology, and meteorology in a tropical forest during two significant ENSO events that brought abnormally wet conditions (2008–2009 La Niña) and drought (2015–2016 El Niño) to observations during non-ENSO years. To learn more about the mechanisms driving seasonal and interannual changes in photosynthesis we calculated different ecological indicators of vegetation response (e.g.: *Pc* and *Gs*), performed regression analysis and implemented a gross ecosystem productivity model. We report the long term trends in photosynthesis, ecosystem respiration, environmental variables and forest function and structure –including stomatal conductance, tree inventories, litter production, and leaf area indices.

3.1. Characterizing meteorology during the La Niña HY2008 and the El Niño HY2015 at K67

At K67 (BR-Sa1), the average seasonal precipitation cycle was characterized by a five month dry-season (July to December) correlated with higher T_{air}, VPD, turbulence, and incoming radiation and lower cloud cover (Fig. S6). Average annual precipitation was 1985 mm where 120 mm corresponded to dry-season rainfall. By contrast, annual precipitation totals during La Niña and El Niño were 2404 and 945 mm, respectively. Wet-season precipitation drove most of the positive anomalies during La Niña and the dry-season was particularly dry and long during El Niño (~seven months with an average of 24 mm month^{-1}). These exceptional values were seen across the basin, with positive and negative $P_{anomaly}$ for the hydrological years July 2008-June 2009 and July 2015-June 2016 (Fig. S1). During both ENSO events seasonal daytime u_*, VPD and T_{air} showed significant deviations from the mean –cool humid air during La Niña, hot conditions with high atmospheric evaporative demand during El Niño. During the 2015–2016 ENSO the all-time relationships between variables (e.g. $T_{air\ \text{daytime}}$ vs. $VPD_{daytime}$, $P_{TRMM\ \text{anomaly}}$ vs. $SW_{in\ CERES\ \text{anomaly}}$, among others) changed; however, they were maintained during La Niña. For example, during the HY2015 drought, $VPD_{daytime}$ increased at a faster rate than the $T_{air\ \text{daytime}}$, indicating extremely dry atmospheric conditions and creating a pressure gradient that promoted leaf water loss (Fig. S7). Furthermore, during the 2015–2016 El Niño, P_{TRMM} decreased more rapidly than incoming radiation ($SW_{in\ CERES}$) (Fig. S8).

3.2. Seasonal carbon fluxes

Observations indicated that during the dry-season, R_{eco} remained at near-constant low levels of ~8 gC m^{-2} d^{-1} and gradually increased as soon as the wet season began, reaching a maximum of 9.6 gC m^{-2} d^{-1} by mid-wet period (Fig. 1c). In contrast, seasonal *GEP* values increased as the dry-season progressed and were maintained at a maximum of ~9 gC m^{-2} d^{-1} mid-dry to mid-wet season. We observed a significant decrease in photosynthesis during both –La Niña (wet-season) and El Niño (all-year) events (Fig. 1a). During HY2015, dry-season reductions in *GEP* were balanced and surpassed by low R_{eco} values, resulting in not statistically significant differences in net carbon flux (*NEE*) from the long term average; however, considerable carbon uptake was observed during the wet season driven by the low R_{eco} (Fig. 1a, c and e). In contrast, during HY2008 lower photosynthetic activity and average seasonal R_{eco} values translated into higher wet-season *NEE* –significant carbon loss (Fig. 1e). While a positive and significant linear correlation existed

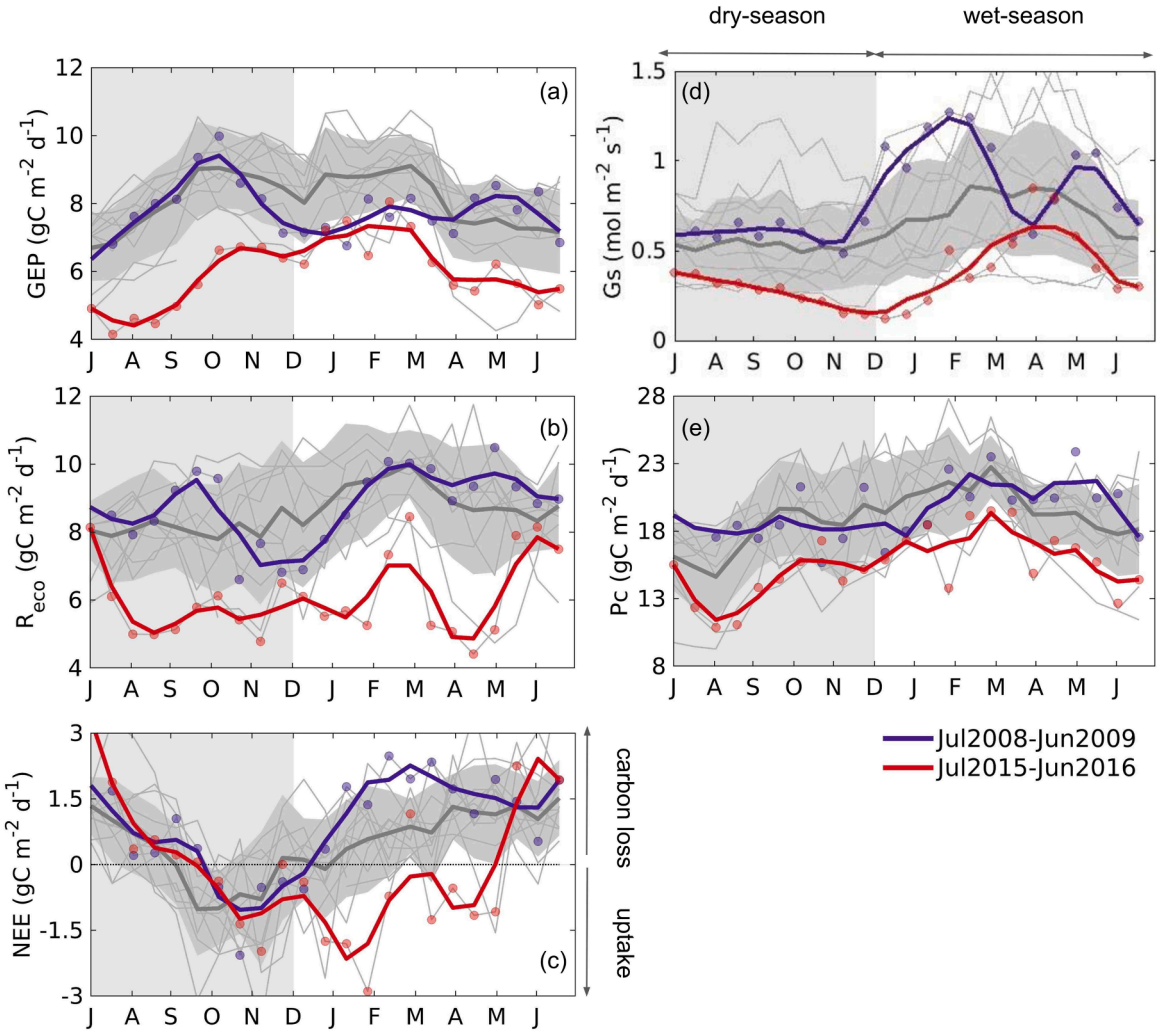

Fig. 1. Santarém K67 (BR-Sa1) seasonal values day-time 16-day of (a) gross ecosystem productivity (*GEP*; gC m^{-2} s^{-1}); (b) ecosystem respiration (R_{eco}; gC m^{-2} s^{-1}); (c) net ecosystem exchange (*NEE*; gC m^{-2} s^{-1}); ecosystem-level canopy stomatal conductance (*Gs*, mol m^{-2} s^{-1}) and (d) photosynthetic capacity (*Pc*; gC m^{-2} s^{-1}). Hydrological years July 2009-June 2010 (blue line), July 2015 – June 2016 (red line) and mean (black line) and standard deviation (dark gray area) of all available observations (2002–2006, 2008–2013 and 2015–2020). July-November gray-shaded area is the average dry season defined as rainfall < 100 mm month^{-1} using satellite-derived measures of precipitation.

between *GEP* and R_{eco}, the 2008–2009 La Niña event saw R_{eco} increasing at a faster than *GEP,* and the relation was not significant during the drought – primarily attributed to the small magnitude of the slope – despite an increase in *GEP* during the HY2015 wet season, R_{eco} remained low (Fig. 2g).

The *GEP* and R_{eco} values observed during El Niño drought remained abnormally low even after rainfall resumed – 2015 to 2018 (Fig. S13). However, trends in *NEE* did not suggest a departure from the all-time average after HY2015.

3.3. Environmental controls on seasonal carbon fluxes

We observed a significant negative correlation between seasonal R_{eco} and $T_{air\ daytime}$, as well as to $VPD_{daytime}$ and a positive relationship with P_{TRMM} for all available observations. Drought conditions, high *VPD* and T_{air}, translated into accelerated reductions in carbon efflux (Fig. 2) and the intercept between R_{eco} and P_{TRMM} changed during the El Niño event. When there was no precipitation during HY2015, R_{eco} was ~6 gC m^{-2} d^{-1} –lower than the all-time mean of ~8 gC m^{-2} d^{-1} (Fig. S10).

Hourly photosynthetic activity at saturated light showed to be controlled by *VPD* rather than T_{air} or soil moisture (*CWD* as proxy) –*GEP* linearly decreased as atmospheric evaporative demand increased (Fig. S9). However, at a seasonal scale, the relationship between photosynthesis and *VPD* was non-statistically significant, nor were the all-time regressions between *GEP* and T_{air} or *Rn* (Fig. 2). By contrast, during the 2015–2016 ENSO, environmental drivers were significantly correlated with seasonal values of photosynthesis –increasing temperature, radiation and atmospheric demand correlated with lower *GEP* (R^2

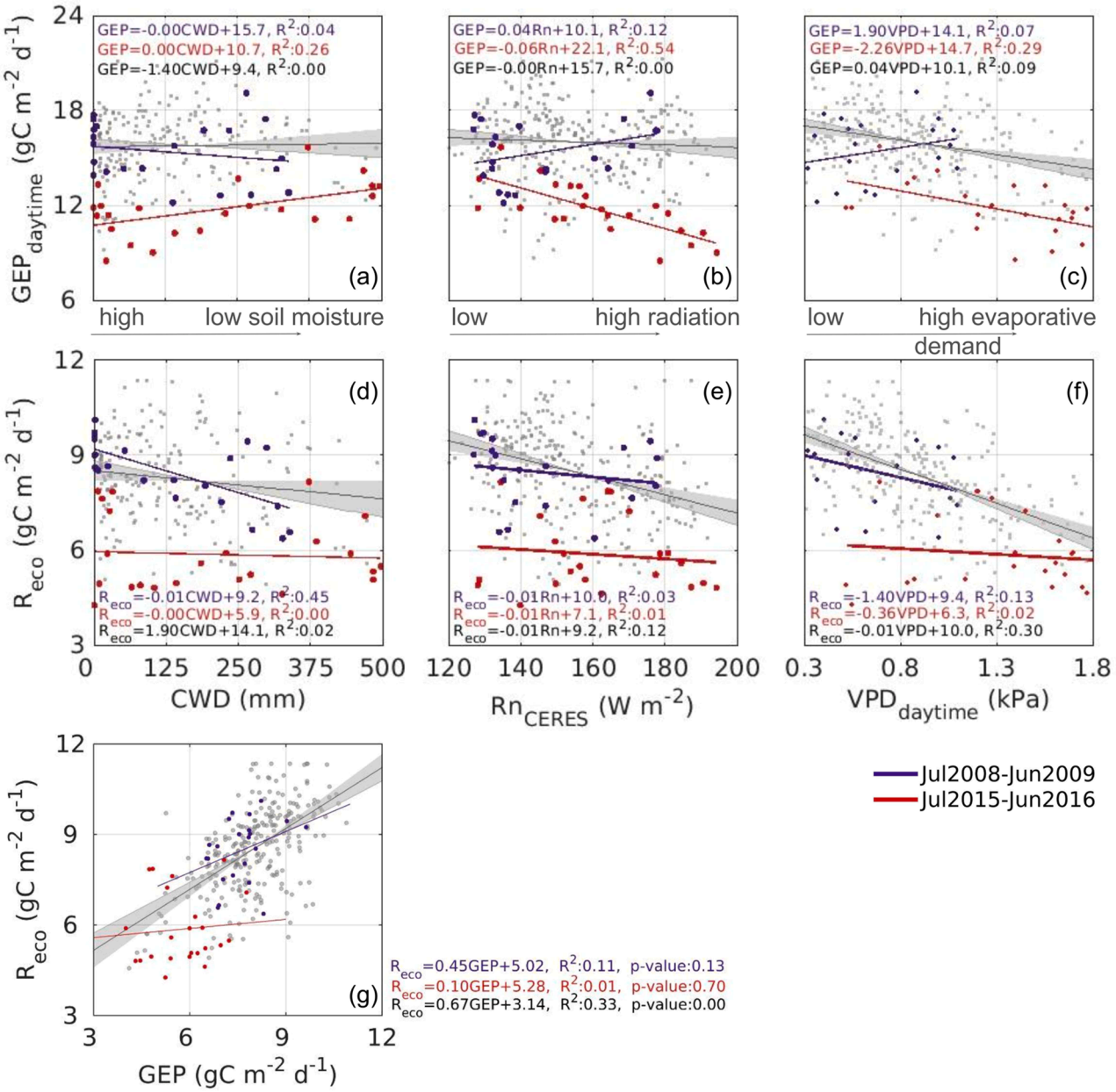

Fig. 2. Santarém K67 (BR-Sa1) linear regression between daytime 16-day gross ecosystem productivity (GEP_{day}; gC m^{-2} d^{-1}) to (a) cumulative water deficit (CWD; mm), (b) satellite derived (CERES) all-sky net radiation (Rn_{CERES}; W m^{-2}) and (c) daytime vapor pressure deficit ($VPD_{daytime}$; kPa). Regression ecosystem respiration (R_{eco}; gC m^{-2} d^{-1}) and (d) CWD, (e) Rn_{CERES} and (f) $VPD_{daytime}$ and (g) gross ecosystem productivity (*GEP;* gC m^{-2} d^{-1}) (includes day and nighttime observations). Hydrological years July 2009-June 2010 (blue line and dots), July 2015 – June 2016 (red line and dots) and mean (gray line and dots) of all available observations (2002–2006, 2008–2013 and 2015–2020). The 95 % confidence intervals for regression coefficient estimates as gray areas.

= 0.20, 0.53, 0.27, respectively, p-values <0.001). Although increasing water deficit conditions (*CWD*) translated into higher $GEP_{daytime}$ during the drought period, photosynthetic activity (intercept and overall values) was significantly lower than the all-time regression (Fig. 2).

To isolate the effect of the different environmental controls on photosynthesis during both ENSO events we used an Light-use Efficiency *GEP* model (Fig. S16-S18). At K67 (BR-Sa1), photosynthesis was driven by biotic factors (here represented by LUE_{ref}), incoming light (including day length), *VPD*, T_{air}, and light quality (diffuse/direct radiation, *CI* as proxy). Our GEP_{model} showed reductions in photosynthesis during the La Niña were driven by low values of *PAR* and phenology (LUE_{ref} as proxy). By contrast, El Niño low photosynthetic activity was driven by lower photosynthetic capacity with a moderate contribution from high *VPD* values (Fig. S18) (see SI Section 5).

3.4. Biological controls on seasonal carbon fluxes

Leaf phenology metrics such as leaf abscission and production, and *Pc* have closely related seasonal cycles. During the dry season high values of leaf litter fall were balanced by high leaf-flush activity ($NPP_{leaf\text{-}flush}$) – this resulted in a high leaf area index ($LAI_{\alpha PAR}$). $Litter_{leaf}$ was negatively correlated to *Pc*. By contrast, elevated values of leaf quality (α_{AM}) and a second peak in leaf quantity (LAI_{fPAR}) observed during the mid-wet to mid-dry season (October-March) (Fig. 3) coincided with increasing photosynthetic capacity (*Pc*) (Fig. 1). The fast photosynthetic response at low light levels (α_{AM}) observed during El Niño dry-season was offset by lower values of photosynthesis at saturated light (P_{nmax}) (Fig. 3 and S14).

Here, we report an increase in $Litter_{leaf}$ and $Litter_{all}$ and a decrease in *LAI* during the wet season of the 2015–2016 ENSO. Our HY2015 $NPP_{leaf\text{-}flush}$ model showed short lived higher leaf production during the transition from dry to wet season (Fig. 3) –not enough to increase total *LAI* values. Moreover, wet-season El Niño reductions in leaf quantity were accompanied by a decrease in the quantum yield of assimilation (α_{AM}) –which describes leaf quality– after an-all time high observed at the beginning of the HY2015 (July-December dry season). After the drought ended and rainfall resumed, P_{nmax} increased and remained at levels above the all-time average (Fig. S14). Leaf photosynthetic response to light showed no significant short or long-term change related to La Niña.

Leaf quantity and quality were significantly low after the wet-season of the 2015–2016 El Niño drought and subsequent years, with α_{AM} values decreasing from December 2015 onward and $LAI_{\alpha PAR}$: from HY2015 to HY2018 (Fig. S14). Unleashing long-term changes in phenology (*Pc*) accompanied by variations in forest physiology, here represented by lower *Gs*, and by higher *VPD* and T_{air} values from HY2015 to HY2018, despite precipitation resumed in 2017 (monthly rainfall was comparable to the climatic mean) (Fig. 4, S11 to S13). The EVI_{sza15} (proxy for *Pc* –leaf quantity and quality) confirmed a significant and sustained reduction in photosynthetic capacity at K67 (BR-Sa1) during the drought – EVI_{sza15} values reached the ~20-year record minima (Fig. 4).

We observed other significant forest structure changes at our study site during HY2015, with higher mortality during and after the drought event (September 2015 and 2017 inventories) – most of the total biomass reductions (kg m^{-2} yr^{-1}) driven by the loss of smaller individuals (diameter, DBH <35 cm) from a few softwood, mid-canopy, shallow-rooted species (preliminary analysis from a small sample). Reduced growth was substantial for all trees in the 2015 inventory (Fig. S15). After the 2015–2016 El Niño, high mortality and slow growth of small trees (DBH <35 cm) translated into slightly reduced above ground biomass estimates for the 2017 forest inventory. By contrast, 2009 biometry measurements (after La Niña) showed reduced mortality and higher growth for large trees (DBH >55 cm) (Fig. 4 and S15).

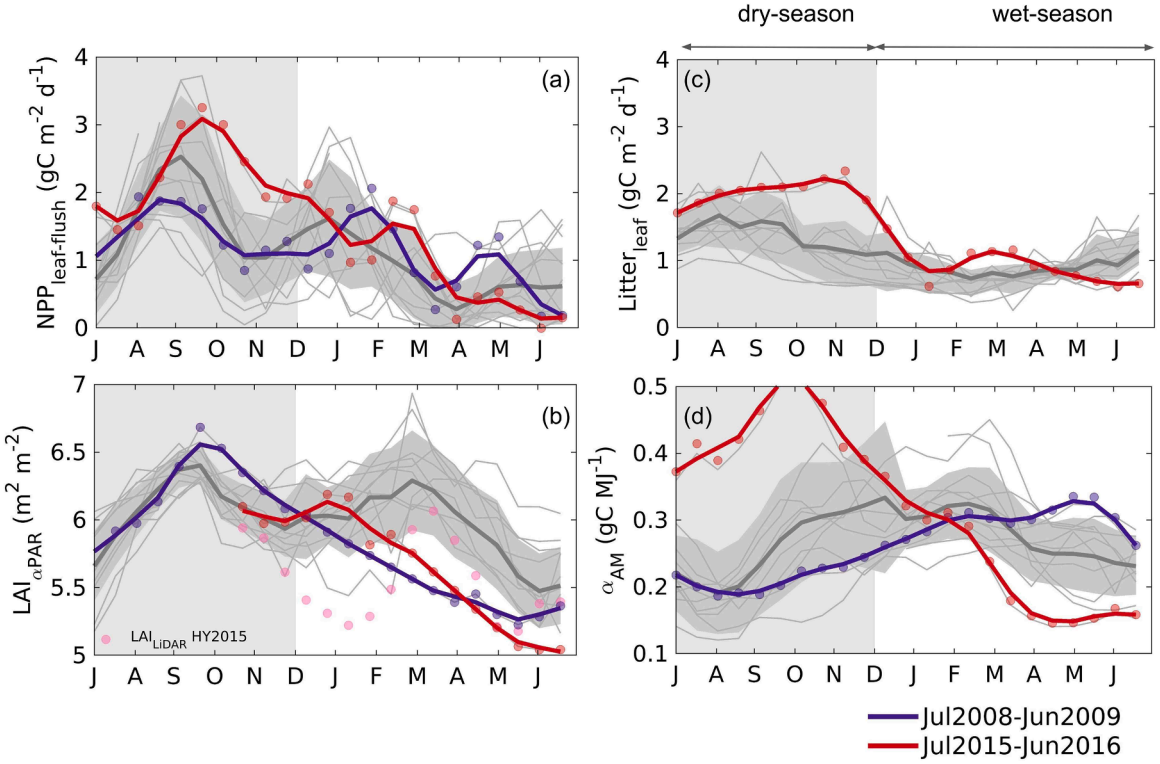

Fig. 3. Santarém K67 seasonal values day-time 16-day of (a) net primary productivity allocated as leaf production ($NPP_{leaf\text{-}flush}$; gC m^{-2} d^{-1}); (b) leaf area index from photosynthetic active radiation ($LAI_{\alpha PAR}$; m^2 m^{-2}) and from LiDAR measurements (LAI_{LiDAR} m^2 m^{-2}); (c) leaf-fall ($Litter_{all}$; gC m^{-2} d^{-1}) and (d) quantum yield of assimilation (α_{AM}; gC MJ^{-1}). Hydrological years July 2009-June 2010 (blue line) and July 2015 – June 2016 (red line). Fine dark gray lines indicate individual hydrological years, their average (black line) and mean ± standard deviation (dark gray area) based on all available observations (2002–2006, 2008–2013 and 2015–2020). July-November light gray-shaded area is the average dry season defined as rainfall < 100 mm $month^{-1}$ using satellite-derived measures of precipitation.

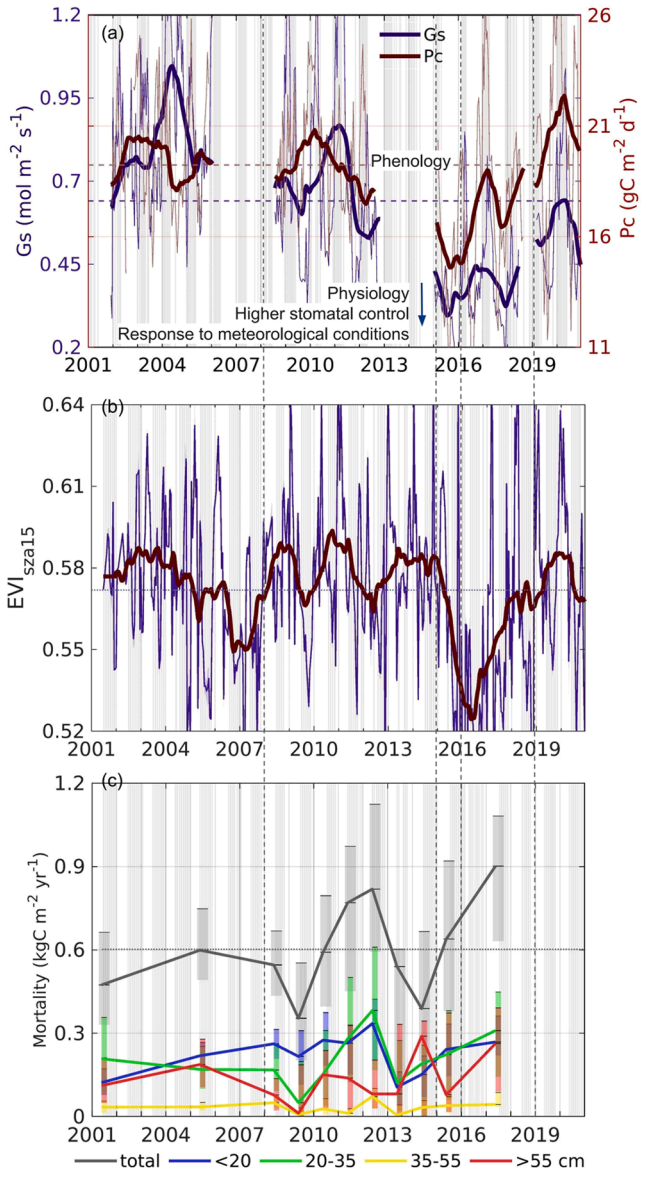

Fig. 4. Santarém K67 (BR-Sa1) seasonal 16-day values of day-time ecosystem-level canopy conductance (Gs/Gs_{max}) and photosynthetic capacity (Pc/Pc_{max}) as a fraction of their maxima. Mean of all Gs/Gs_{max} available observations (2002–2006, 2008–2013 and 2015–2020) (blue line), standard deviation (shaded light blue area) and deseasonalized –long-time trends obtained by applying a seasonal adjustment (removing the seasonal component) and using a stable seasonal filter (annual moving average) (dark thick blue line). The average Pc/Pc_{max} (red lines), standard deviation (red shaded area) and deseasonalized time series (dark thick red line). (b) Enhanced vegetation index (EVI) from the MCD43C1 v006 CMG daily product (Schaaf and Wang, 2015; Schaaf et al., 2002) bidirectional reflectance distribution function (BRDF) adjusted reflectance calculated for observer at nadir and solar zenith angle at 15° (EVI_{sza15}). (c) Tree mortality values from annual forest inventories (*Mortality*; kgC m^{-2} $year^{-1}$), here presented per size class <20 cm diameter breast height (DBH) trees (blue bars and lines), 20–35 cm DBH (green bars and lines), 35–55 cm DBH (yellow bars and lines), stems >55 cm DBH (red bars and lines), and total mortality (gray bars and lines). Bars defined by the expectation and the 25 and 75 % confidence intervals calculated by bootstrapping combined with random attribution (assuming the year when the individual went missing was different than the year of the sample) (Longo, 2014). Gray-shaded areas are dry season conditions defined as satellite-derived precipitation < 100 mm $month^{-1}$.

4. Discussion

The ability to maintain long-term EC flux measurements and forest dynamics inventories is critical to the task of scaling mechanisms from individuals to ecosystems. Across Amazonia two ENSO events brought extreme precipitation, temperatures and moisture regimes. At K67 Tapajós National Forest the 2008–2009 La Niña was characterized by high rainfall, low temperature and *VPD* during the wet-season and the 2015–2016 El Niño brought drought conditions, offering the opportunity to contrast tropical forest response to climatic extremes and recovery times. Our results show: (1) an increase in carbon loss during the wet event, when high values of *NEE* were driven by low photosynthetic activity induced by low incoming radiation, this despite to high *Gs* values; (2) overall, there was either short-lived uptake or carbon neutrality throughout the drought period, attributed to the simultaneous suppression of both productivity and respiration, (3) reductions in photosynthesis were linked to loss of vegetation capacity (both –leaf quantity and quality) during the dry-season and reductions in canopy stomatal conductance response to high *VPD*. (4) Low *Gs* values reported during El Niño, and a few years after the drought can be related to significant changes in leaf physiology– increasing vegetation controls limiting transpiration and photosynthetic activity. Here we discuss these results in the context of environmental and phenological drivers and its significance when determining forest resilience and susceptibility to climate anomalies.

4.1. What is the effect of extreme climatic events on seasonal carbon flux components (photosynthesis and respiration)?

Whereas La Niña's reductions in photosynthetic activity were not as significant as those observed during the El Niño drought, the 2008–2009 *GEP* drove the HY2008 carbon imbalance, here represented by high *NEE* values. By contrast the low ecosystem respiration (R_{eco}) drove the short lived uptake during the El Niño. Where R_{eco} encompasses autotrophic respiration (vegetation growth, maintenance, and reproduction) (R_a), and heterotrophic respiration (decomposition) (R_h). Therefore, we could infer from the positive correlation between *GEP* and R_{eco} during non-ENSO years (Fig. 2g) and previous estimates at a nearby forest ($R_a = 0.72R_{eco}$ and $R_h = 0.28R_{eco}$) (Miller et al., 2011) that at K67, the CO_2 efflux was dominated by autotrophic respiration. However, the regression *GEP* v. R_{eco} changed during both ENSO events, suggesting that under abnormally dry or wet conditions heterotrophic respiration may have had a more significant contribution to R_{eco}, either through suppression or enhancement (Fig. 2h). During La Niña, increased soil moisture may elevate rates of decomposition (Giweta, 2020), while the abnormally low photosynthetic activity values during El Niño may have been balanced by equally low values of R_a and consequently R_{eco}. During the drought, across the Amazon, leaf measurements, live and dead woody tissue, and soil respiration revealed that although leaf dark respiration was maintained, the wood and leaves efflux was reduced as *LAI* declined, as well as the necromass decomposition diminished (Meir et al., 2008).

4.2. Does the seasonal relationship between meteorological values and GEP, R_{eco} and NEE changes under abnormally dry or wet conditions?

Although photosynthesis decreased during the El Niño, the corresponding values of T_{air} and *VPD* at which maximum *GEP* values were observed, increased reaching values up to 30.6 C and 2.2 kPa. Our dataset confirms that high *VPD* values are the main driver of hourly *GEP* reductions rather than T_{air} (as in Smith et al. (2020)) and/or soil water content (*CWD* as proxy) (opposite to modeling work by Fang et al. (2021)). Linked to the 2015–2016 ENSO and the next three years, we observed a decoupling of T_{air} vs. *VPD* – which shows a faster increase in air dryness that may be reflected in the lower *Gs* values. Moreover, our observations do not show signs of higher *GEP* due to increased radiation

nor T_{air}. The reported drying and warming trends observed at the Tapajós region, along with vegetation responses, highlight that the predicted enhanced productivity due to CO_2 enrichment or high temperature may not be applicable to all tropical forests. Fertilization effects can ***only*** occur if the increase in T_{air} is moderate and accompanied by excess precipitation (Gustafson et al., 2017).

At K67 (BR-Sa1), the rise in forest mortality during and after the El Niño was mainly driven by small individuals (DBH<35 cm). This contrasts with results from the nearby *Seca Floresta* rain out experiment which showed mortality of large adult trees as driving canopy gap formation and declines in litterfall production (Brando et al., 2006; Nepstad et al., 2007). While the experimental drought excluded 60 % of throughfall (~3-years) (Nepstad et al., 2002), here we report how increased *VPD,* rather than plant available water drove reductions in *GEP* –perhaps explaining differences in mortality. Both the partial throughfall exclusion experiment and the ENSO 2015–2016 showed reductions in growth of small individuals. Biomass loss and reduced growth are clear indications of vegetation stress and forest disturbance –flux (e.g. *GEP*), environmental (e.g. *VPD*) and other ground and remote sensing measurements (e.g. *EVI*) data signaled a slow recovery (+3 years).

4.3. Vegetation strategies and carbon flux during extreme events

Radiation and leaf phenology contributed to lower photosynthetic activity throughout the La Niña wet event. Similarly, we showed how Pc/LUE_{ref} and $VPD_{daytime}$ drove reductions in *GEP* during the drought. Where the photosynthetic capacity (*Pc* and greenness indices) are driven by both the quality (e.g. age, A_{max}) and quantity of leaves (e.g. *LAI*). Here, we report long-term losses in leaf **quantity** (LAI_{aPAR}) during and after the El Niño event. Moreover, at K67 Smith et al. (2019) showed how the seasonal changes in the vertical distribution of *LAI* were more significant than the total change; thus lower canopy *LAI* decreased as the upper canopy *LAI* increased during the dry season –their observations showed seasonal trends magnified during the 2015–2016 El Niño. Interpreting quantum yield of assimilation (α_{AM}) as a measure of leaf **quality**, we report a significant increase during the dry-season drought –coinciding with leaf-flush and increased upper canopy *LAI* –this may be related to the fact that top canopy (sun-exposed sacrificial) leaves subjected to greater stress (light, atmospheric evaporative demand, temperature and wind) show lower quality (thicker, smaller, and have less chlorophyll) compared to understory shaded leaves (Souza et al., 2018). The higher top canopy *LAI* coincided with low P_{nmaxAM}. By contrast, during the El Niño "wet-season", possible feedback effects (reduction in *ET*) added to the lack of precipitation, which translated into higher *VPD* and T_{air}, lower canopy conductance (leaf physiological response, as in low α_{AM}) and resulted in low photosynthetic activity.

We could anticipate other changes related to the timing of different phenological cycles, for example, favoring species that flush at a different times of the year or going into senescence during the dry-season (Scranton and Amarasekare, 2017). Alternatively, as Barros et al. (2019) found at our study site, there was a distinct (less diverse) community assembly of hydraulic traits and taxa associated with high drought tolerance (when compared to a less seasonal equatorial forest site, Manaus, K34). These K67 (BR-Sa1) species were characterized by greater xylem embolism resistance and were able to maintain a similar hydraulic safety margin during the peak of the drought (December 2015) compared to the previous year (Barros et al., 2019). Indeed, at ecosystem level we observed the sustained abnormally low *Gs, ET,* α_{AM}, and photosynthetic activity from November 2015 to March 2016; however, the long term *Gs,* α_{AM}, and *Pc* indicated longlasting phenological and physiological changes, and the 2017 forest inventories indicated a significantly higher than usual mortality in small size classes – future work will identify the species that would have been subject to embolism and death and compare their hydraulic traits to those of individuals that survived and/or did thrive.

5. Conclusion

Across the Amazon basin over the past few decades, rainfall data suggest an increase in the frequency of anomalously severe floods and droughts, and the intensification of the hydrological cycle, where dry season precipitation has slightly decreased, and wet season and annual mean precipitation have increased (Gloor et al., 2015). However, land surface model simulations of biomass and productivity have shown difficulties in replicating the strong effect that climate extremes exert across short time scales, thus long-term observations and measurements of tropical forest dynamics during drought are scarce (Castanho et al., 2016). Here, we have shown the other side of drought, when high precipitation, **low incoming radiation, and phenological changes,** drove ***short-lived*** carbon losses, indicating that light and vegetation capacity can significantly limit productivity. Moreover, long-term measurements of tropical forest dynamics demonstrate how light drives dry-season increases in photosynthesis and key phenological cycles (e.g. leaf flush and abscission -forest "green-up") (Huete et al., 2006; Hutyra et al., 2007; Restrepo-Coupe et al., 2013; Saleska et al., 2007; Wu et al., 2016). Yet, we have shown how anomalous ***dry periods*** have ***long-term*** (lasting three to four years after drought) consequences on site climate (atmospheric demand and T_{air}), vegetation physiology (*Gs,* P_{nmaxAM} and α_{AM}), phenology (*Pc*) and structure (LAI_{aPAR}, and mortality). Moreover, our results point to water stress –driven by *VPD* rather than T_{air}, soil moisture (*CWD* as proxy), nor to access to groundwater (~100 m depth (Nepstad et al., 2002)), as a key driver not only of photosynthesis, but of ecosystem respiration, decreasing tree performance, and increasing mortality, possibly resulting on altering forest functional diversity (Barros et al., 2019; Betts et al., 2004, Brum et al., 2018; Castanho et al., 2016; Cox et al., 2004; Phillips et al., 2009; Zhang et al., 2015) with significant consequences for ecosystem carbon exchange, the effect of fertilization and forest resilience.

CRediT authorship contribution statement

Natalia Restrepo-Coupe: Writing – review & editing, Writing – original draft, Visualization, Validation, Software, Methodology, Investigation, Formal analysis, Data curation, Conceptualization. **Kleber Silva Campos:** Methodology, Data curation. **Luciana F. Alves:** Methodology, Investigation, Data curation, Writing – original draft, Writing – review & editing. **Marcos Longo:** Data curation, Investigation, Methodology, Writing – original draft, Writing – review & editing. **Kenia T. Wiedemann:** Data curation. **Raimundo Cosme de Oliveira:** Supervision, Resources, Project administration, Investigation, Funding acquisition. **Luiz E.O.C. Aragao:** Resources, Data curation. **Bradley O. Christoffersen:** Methodology, Data curation. **Plinio B. Camargo:** Resources, Data curation. **Adelaine M.e S. Figueira:** Resources, Data curation. **Maurício Lamano Ferreira:** Data curation. **Rafael S. Oliveira:** Writing – review & editing, Resources, Project administration, Data curation. **Deliane Penha:** Data curation. **Neill Prohaska:** Data curation. **Alessandro C. da Araujo:** Resources. **Bruce C. Daube:** Methodology, Investigation, Data curation. **Steven C. Wofsy:** Writing – review & editing, Conceptualization. **Scott R. Saleska:** Writing – review & editing, Supervision, Project administration, Methodology, Investigation, Funding acquisition, Conceptualization.

Declaration of competing interest

The authors declare that they have no known competing financial interests or personal relationships that could have appeared to influence the work reported in this paper.

Data availability

Data submited at Ameriflux and DRYAD repository. Code available at GitHub

Data Availability Statement

Hourly eddy covariance data presented and analyzed here (from 2002 to 2020) are posted at the Ameriflux K67 (BR-Sa1) repository (https://ameriflux.lbl.gov/sites/siteinfo/BR-Sa1). Seasonal (16-day averages) have also been uploaded into the DRYAD repository: https://datadryad.org/stash/dataset/doi:10.5061/dryad.d51c5b08g. The code for data analysis is available at https://github.com/nataliacoupe/k67.eddy.covariance. Litter and ground aboveground biomass data can be accessed from the ORNL DAAC LBA-ECO https://daac.ornl.gov/LBA/guides/CD10_Litter_Tapajos.html, https://daac.ornl.gov/cgi-bin/dsviewer.pl?ds_id=854, and upon request.

Acknowledgments

This research was funded by awards over the life of eddy flux measurements in the Tapajós National forest, including from the Brazilian-led Large scale Biosphere Atmosphere experiment in Amazonia (under whose auspices we established tower flux measurements in 2001) with funding contributions over the years from National Aeronautics and Space Administration (NASA) LBA investigation CD-32, NASA ROSES (Award #NNX17AF65G), the GOAmazon project, jointly funded by the U.S. Department of Energy (DOE) (Award #DE-FOA-0000919), and the Brazilian science foundations FAPESP (13/50533–5) and FAPEAM; and awards from the U.S. National Science Foundation (NSF), including PIRE (Award #0730305), RAPID (#1622721) 'IsoTraits' (#1754803 and #1753973), Other Side of Drought (#1950080), and Cascade "Hydronomics" (#2106804). The authors would like to thank our faithful collaborators: Janitoni (Louro) Lima da Costa, Dr. Mauro Brum, Dr. Marielle N. Smith, Dr. Lina Mercado, Daniel Amaral, David Garces, Sky Dominguez and past and present technical personnel. We acknowledge the contribution of Dr. Umberto Lombardo for providing the map of legal Amazonia. First author acknowledges the support from Professor Alfredo R. Huete at University Technology Sydney and the City of Toronto Children and Human Services, Dr. Debra Wunch, and the Department of Physics at the University of Toronto.

Supplementary materials

Supplementary material associated with this article can be found, in the online version, at doi:10.1016/j.agrformet.2024.110037.

References

Ahlström, A., Schurgers, G., Arneth, A., Smith, B., 2012. Robustness and uncertainty in terrestrial ecosystem carbon response to CMIP5 climate change projections. Environ. Res. Lett. 7, 1–9. https://doi.org/10.1088/1748-9326/7/4/044008.

Allen, C.D., Macalady, A.K., Chenchouni, H., Bachelet, D., McDowell, N., Vennetier, M., Kitzberger, T., Rigling, A., Breshears, D.D., Hogg, E.H., Ted Gonzalez, P., Fensham, R., Zhang, Z., Castro, J., Demidova, N., Lim, J.H., Allard, G., Running, S. W., Semerci, A., Cobb, N., 2010. In: A global overview of drought and heat-induced tree mortality reveals emerging climate change risks for forests. For. Ecol. Manag., Adaptation of Forests and Forest Management to Changing ClimateSelected papers from the conference on "Adaptation of Forests and Forest Management to Changing Climate with Emphasis on Forest Health: A Review of Science, Policies and Practices. Umeå, Sweden, 259, pp. 660–684. https://doi.org/10.1016/j.foreco.2009.09.001. August 25-28, 2008.

Alves, L.F., Longo, M., Stark, S.C., Ferreira, M.L., da Costa, C.F.G., Aragão, L.E., Saleska, S.R., Oliveira Junior, R.C., Camargo, P.B.D., 2018. Multi-year Legacy Impacts Following Droughts in a Seasonal Amazon Forest 53.

Amigo, I., 2020. When will the Amazon hit a tipping point? Nature 578, 505–507. https://doi.org/10.1038/d41586-020-00508-4.

Aragão, L.E.O.C., Malhi, Y., Roman-Cuesta, R.M., Saatchi, S., Anderson, L.O., Shimabukuro, Y.E., 2007. Spatial patterns and fire response of recent Amazonian droughts. Geophys. Res. Lett. 34, 5. https://doi.org/10.1029/2006GL028946.

Barichivich, J., Gloor, E., Peylin, P., Brienen, R.J.W., Schöngart, J., Espinoza, J.C., Pattnayak, K.C., 2018. Recent intensification of Amazon flooding extremes driven by strengthened Walker circulation. Sci. Adv. https://doi.org/10.1126/sciadv.aat8785.

Barros, F., de, V., Bittencourt, P.R.L., Brum, M., Restrepo-Coupe, N., Pereira, L., Teodoro, G.S., Saleska, S.R., Borma, L.S., Christoffersen, B.O., Penha, D., Alves, L.F., Lima, A.J.N., Carneiro, V.M.C., Gentine, P., Lee, J.E., Aragão, L.E.O.C., Ivanov, V., Leal, L.S.M., Araujo, A.C., Oliveira, R.S., 2019. Hydraulic traits explain differential responses of Amazonian forests to the 2015 El Niño-induced drought. New. Phytol. 223, 1253–1266. https://doi.org/10.1111/nph.15909.

Bennett, A.C., Rodrigues de Sousa, T., Monteagudo-Mendoza, A., Esquivel-Muelbert, A., Morandi, P.S., Coelho de Souza, F., Castro, W., Duque, L.F., Flores Llampazo, G., Manoel dos Santos, R., Ramos, E., Vilanova Torre, E., Alvarez-Davila, E., Baker, T.R., Costa, F.R.C., Lewis, S.L., Marimon, B.S., Schietti, J., Burban, B., Berenguer, E., Araujo-Murakami, A., Restrepo Correa, Z., Lopez, W., Delgado Santana, F., Viscarra, L.J., Elias, F., Vasquez Martinez, R., Marimon-Junior, B.H., Galbraith, D., Sullivan, M.J.P., Emilio, T., Prestes, N.C.C.S., Barlow, J., Alencar Fagundes, N.C., Almeida de Oliveira, E., Alvarez Loayza, P., Alves, L.F., Aparecida Vieira, S., Andrade Maia, V., Aragão, L.E.O.C., Arets, E.J.M.M., Arroyo, L., Bánki, O., Baraloto, C., Barbosa Camargo, P., Barroso, J., Bento da Silva, W., Bonal, D., Borges Miranda Santos, A., Brienen, R.J.W., Brown, F., Castilho, C.V., Cerruto Ribeiro, S., Chama Moscoso, V., Chavez, E., Comiskey, J.A., Cornejo Valverde, F., Dávila Cardozo, N., de Aguiar-Campos, N., de Oliveira Melo, L., del Aguila Pasquel, J., Derroire, G., Disney, M., do Socorro, M., Dourdain, A., Feldpausch, T.R., Ferreira, J., Forni Martins, V., Gardner, T., Gloor, E., Gutierrez Sibauty, G., Guillen, R., Hase, E., Hérault, B., Honorio Coronado, E.N., Huaraca Huasco, W., Janovec, J.P., Jimenez-Rojas, E., Joly, C., Kalamandeen, M., Killeen, T.J., Lais Farrapo, C., Levesley, A., Lizon Romano, L., Lopez Gonzalez, G., Maës dos Santos, F.A., Magnusson, W.E., Malhi, Y., Matias de Almeida Reis, S., Melgaço, K., Melo Cruz, O.A., Mendoza Polo, I., Montañez, T., Morel, J.D., Núñez Vargas, M.P., Oliveira de Araújo, R., Pallqui Camacho, N.C., Parada Gutierrez, A., Pennington, T., Pickavance, G.C., Pipoly, J., Pitman, N.C.A., Quesada, C., Ramirez Arevalo, F., Ramírez-Angulo, H., Flora Ramos, R., Richardson, J.E., Rodrigo de Souza, C., Roopsind, A., Schwartz, G., Silva, R.C., Silva Espejo, J., Silveira, M., Singh, J., Soto Shareva, Y., Steininger, M., Stropp, J., Talbot, J., ter Steege, H., Terborgh, J., Thomas, R., Valenzuela Gamarra, L., van der Heijden, G., van der Hout, P., Zagt, R., Phillips, O.L., 2023. Sensitivity of South American tropical forests to an extreme climate anomaly. Nat. Clim. Change 13, 967–974. https://doi.org/10.1038/s41558-023-01776-4.

Betts, R.A., Cox, P.M., Collins, M., Harris, P.P., Huntingford, C., Jones, C.D., 2004. The role of ecosystem-atmosphere interactions in simulated Amazonian precipitation decrease and forest dieback under global climate warming. Theor. Appl. Climatol. 78, 157–175. https://doi.org/10.1007/s00704-004-0050-y.

Bonal, D., Burban, B., Stahl, C., Wagner, F., Hérault, B., 2016. The response of tropical rainforests to drought—Lessons from recent research and future prospects. Ann. For. Sci. 73, 27–44. https://doi.org/10.1007/s13595-015-0522-5.

Botía, S., Komiya, S., Marshall, J., Koch, T., Gałkowski, M., Lavric, J., Gomes-Alves, E., Walter, D., Fisch, G., Pinho, D.M., Nelson, B.W., Martins, G., Luijkx, I.T., Koren, G., Florentie, L., Carioca de Araújo, A., Sá, M., Andreae, M.O., Heimann, M., Peters, W., Gerbig, C., 2022. The CO2 record at the Amazon Tall Tower Observatory: A new opportunity to study processes on seasonal and inter-annual scales. Glob. Change Biol. 28, 588–611. https://doi.org/10.1111/gcb.15905.

Brando, P., Ray, D., Nepstad, D., Cardinot, G., Curran, L.M., Oliveira, R., 2006. Effects of partial throughfall exclusion on the phenology of Coussarea racemosa (Rubiaceae) in an east-central Amazon rainforest. Oecologia 150, 181–189. https://doi.org/10.1007/s00442-006-0507-z.

Brando, P.M., Soares-Filho, B., Rodrigues, L., Assunção, A., Morton, D., Tuchschneider, D., Fernandes, E.C.M., Macedo, M.N., Oliveira, U., Coe, M.T., 2020. The gathering firestorm in southern. Amazonia. Sci. Adv. 6, eaay1632. https://doi.org/10.1126/sciadv.aay1632.

Brockwell, P.J., Davis, R.A., 2002. Introduction to time series and forecasting. Springer Texts in Statistics, 2nd ed. Springer, New York.

Brum, M., Vadeboncoeur, M.A., Ivanov, V., Asbjornsen, H., Saleska, S., Alves, L.F., Penha, D., Dias, J.D., Aragão, L.E.O.C., Barros, F., Bittencourt, P., Pereira, L., Oliveira, R.S., 2018. Hydrological niche segregation defines forest structure and drought tolerance strategies in a seasonal Amazon forest. J. Ecol. https://doi.org/10.1111/1365-2745.13022.

Castanho, A.D., de, A., Galbraith, D., Zhang, K., Coe, M.T., Costa, M.H., Moorcroft, P., 2016. Changing Amazon biomass and the role of atmospheric CO2 concentration, climate, and land use. Glob. Biogeochem. Cycles 30, 18–39. https://doi.org/10.1002/2015GB005135.

Chavana-Bryant, C., Malhi, Y., Wu, J., Asner, G.P., Anastasiou, A., Enquist, B.J., Cosio Caravasi, E.G., Doughty, C.E., Saleska, S.R., Martin, R.E., Gerard, F.F., 2016. Leaf aging of Amazonian canopy trees as revealed by spectral and physiochemical measurements. New. Phytol. https://doi.org/10.1111/nph.13853.

Chave, J., Réjou-Méchain, M., Búrquez, A., Chidumayo, E., Colgan, M.S., Delitti, W.B.C., Duque, A., Eid, T., Fearnside, P.M., Goodman, R.C., Henry, M., Martínez-Yrízar, A., Mugasha, W.A., Muller-Landau, H.C., Mencuccini, M., Nelson, B.W., Ngomanda, A., Nogueira, E.M., Ortiz-Malavassi, E., Pélissier, R., Ploton, P., Ryan, C.M., Saldarriaga, J.G., Vieilledent, G., 2014. Improved allometric models to estimate the aboveground biomass of tropical trees. Glob. Change Biol. 20, 3177–3190. https://doi.org/10.1111/gcb.12629.

Cox, P.M., Betts, R.A., Collins, M., Harris, P.P., Huntingford, C., Jones, C.D., 2004. Amazonian forest dieback under climate-carbon cycle projections for the 21st century. Theor. Appl. Climatol. 78, 137–156. https://doi.org/10.1007/s00704-004-0049-4.

Davidson, E.A., de Araújo, A.C., Artaxo, P., Balch, J.K., Brown, I.F.C., Bustamante, M.M., Coe, M.T., DeFries, R.S., Keller, M., Longo, M., Munger, J.W., Schroeder, W., Soares-Filho, B.S., Souza, C.M., Wofsy, S.C., 2012. The Amazon basin in transition. Nature 481, 321–328. https://doi.org/10.1038/nature10717.

Detto, M., Pacala, S.W., 2022. Plant hydraulics, stomatal control, and the response of a tropical forest to water stress over multiple temporal scales. Glob. Change Biol. 28, 4359–4376. https://doi.org/10.1111/gcb.16179.

Detto, M., Wright, S.J., Calderón, O., Muller-Landau, H.C., 2018. Resource acquisition and reproductive strategies of tropical forest in response to the El Niño–Southern Oscillation. Nat. Commun. 9, 913. https://doi.org/10.1038/s41467-018-03306-9.

Doughty, C.E., Goulden, M.L., 2008. Seasonal patterns of tropical forest leaf area index and CO2 exchange. J. Geophys. Res. 113, 1–12. https://doi.org/10.1029/2007JG000590.

Duffy, P.B., Brando, P., Asner, G.P., Field, C.B., 2015. Projections of future meteorological drought and wet periods in the Amazon. Proc. Natl. Acad. Sci. 112, 13172–13177. https://doi.org/10.1073/pnas.1421010112.

Esquivel-Muelbert, A., Baker, T.R., Dexter, K.G., Lewis, S.L., Brienen, R.J.W., Feldpausch, T.R., Lloyd, J., Monteagudo-Mendoza, A., Arroyo, L., Álvarez-Dávila, E., Higuchi, N., Marimon, B.S., Marimon-Junior, B.H., Silveira, M., Vilanova, E., Gloor, E., Malhi, Y., Chave, J., Barlow, J., Bonal, D., Davila Cardozo, N., Erwin, T., Fauset, S., Hérault, B., Laurance, S., Poorter, L., Qie, L., Stahl, C., Sullivan, M.J.P., ter Steege, H., Vos, V.A., Zuidema, P.A., Almeida, E., Almeida de Oliveira, E., Andrade, A., Vieira, S.A., Aragão, L., Araujo-Murakami, A., Arets, E., Aymard, C.G. A., Baraloto, C., Camargo, P.B., Barroso, J.G., Bongers, F., Boot, R., Camargo, J.L., Castro, W., Chama Moscoso, V., Comiskey, J., Cornejo Valverde, F., Lola da Costa, A. C., del Aguila Pasquel, J., Di Fiore, A., Fernanda Duque, L., Elias, F., Engel, J., Flores Llampazo, G., Galbraith, D., Herrera Fernández, R., Honorio Coronado, E., Hubau, W., Jimenez-Rojas, E., Lima, A.J.N., Umetsu, R.K., Laurance, W., Lopez-Gonzalez, G., Lovejoy, T., Aurelio Melo Cruz, O., Morandi, P.S., Neill, D., Núñez Vargas, P., Pallqui Camacho, N.C., Parada Gutierrez, A., Pardo, G., Peacock, J., Peña-Claros, M., Peñuela-Mora, M.C., Petronelli, P., Pickavance, G.C., Pitman, N., Prieto, A., Quesada, C., Ramírez-Angulo, H., Réjou-Méchain, M., Restrepo Correa, Z., Roopsind, A., Rudas, A., Salomão, R., Silva, N., Silva Espejo, J., Singh, J., Stropp, J., Terborgh, J., Thomas, R., Toledo, M., Torres-Lezama, A., Valenzuela Gamarra, L., van de Meer, P.J., van der Heijden, G., van der Hout, P., Vasquez Martinez, R., Vela, C., Vieira, I.C.G., Phillips, O.L., 2019. Compositional response of Amazon forests to climate change. Glob. Change Biol. 25, 39–56. https://doi.org/10.1111/gcb.14413.

Esteban, E.J.L., Castilho, C.V., Melgaço, K.L., Costa, F.R.C., 2021. The other side of droughts: wet extremes and topography as buffers of negative drought effects in an Amazonian forest. New. Phytol. 229, 1995–2006. https://doi.org/10.1111/nph.17005.

Fang, Y., Leung, L.R., Wolfe, B.T., Detto, M., Knox, R.G., McDowell, N.G., Grossiord, C., Xu, C., Christoffersen, B.O., Gentine, P., Koven, C.D., Chambers, J.Q., 2021. Disentangling the Effects of Vapor Pressure Deficit and Soil Water Availability on Canopy Conductance in a Seasonal Tropical Forest During the 2015 El Niño Drought. J. Geophys. Res. Atmospheres 126, e2021JD035004.

Field, C.B., Jackson, R.B., Mooney, H.A., 1995. Stomatal responses to increased CO2: implications from the plant to the global scale. Plant Cell Environ 18, 1214–1225. https://doi.org/10.1111/j.1365-3040.1995.tb00630.x.

Gamon, J.A., 2015. Reviews and Syntheses: optical sampling of the flux tower footprint. Biogeosciences 12, 4509–4523. https://doi.org/10.5194/bg-12-4509-2015.

Giweta, M., 2020. Role of litter production and its decomposition, and factors affecting the processes in a tropical forest ecosystem: a review. J. Ecol. Environ. 44, 11. https://doi.org/10.1186/s41610-020-0151-2.

Gloor, M., Barichivich, J., Ziv, G., Brienen, R., Schöngart, J., Peylin, P., Cintra, B.B.L., Feldpausch, T., Phillips, O., Baker, J., 2015. Recent Amazon climate as background for possible ongoing and future changes of Amazon humid forests. Glob. Biogeochem. Cycles 29, 1384–1399. https://doi.org/10.1002/2014GB005080.

Gloor, M., Brienen, R.J.W., Galbraith, D., Feldpausch, T.R., Schöngart, J., Guyot, J.L., Espinoza, J.C., Lloyd, J., Phillips, O.L., 2013. Intensification of the Amazon hydrological cycle over the last two decades. Geophys. Res. Lett. 40, 1729–1733. https://doi.org/10.1002/grl.50377.

Goudriaan, J., 1986. A simple and fast numerical method for the computation of daily totals of crop photosynthesis. Agric. For. Meteorol. 38, 249–254. https://doi.org/10.1016/0168-1923(86)90063-8.

Gustafson, E.J., Miranda, B.R., De Bruijn, A.M.G., Sturtevant, B.R., Kubiske, M.E., 2017. Do rising temperatures always increase forest productivity? Interacting effects of temperature, precipitation, cloudiness and soil texture on tree species growth and competition. Environ. Model. Softw. 97, 171–183. https://doi.org/10.1016/j.envsoft.2017.08.001.

Huete, A.R., Didan, K., Shimabukuro, Y.E., Ratana, P., Saleska, S.R., Hutyra, L.R., Yang, W., Nemani, R.R., Myneni, R., 2006. Amazon rainforests green-up with sunlight in dry season. Geophys. Res. Lett. 33, L06405. https://doi.org/10.1029/2005GL025583.

Huffman, G., Bolvin, D., Braithwaite, D., Hsu, K., Joyce, R., Xie, P., 2014. Integrated Multi-satellitE Retrievals for GPM (IMERG), version 6.0. NASA's Precipitation Processing Center [WWW Document]. URL http://arthurhou.pps.eosdis.nasa.gov/gpmdata/(accessed 7.31.20).

Huffman, G.J., Bolvin, D.T., Nelkin, E.J., Wolff, D.B., Adler, R.F., Gu, G., Hong, Y., Bowman, K.P., Stocker, E.F., 2007. The TRMM Multisatellite Precipitation Analysis (TMPA): Quasi-Global, Multiyear, Combined-Sensor Precipitation Estimates at Fine Scales. J. Hydrometeorol. 8, 38–55. https://doi.org/10.1175/JHM560.1.

Hutyra, L.R., Munger, J.W., Saleska, S.R., Gottlieb, E., Daube, B.C., Dunn, A.L., Amaral, D.F., de Camargo, P.B., Wofsy, S.C., 2007. Seasonal controls on the exchange of carbon and water in an Amazonian rain forest. J. Geophys. Res. Biogeosci. 112, 1–16. https://doi.org/10.1029/2006JG000365.

IPCC, 2013. Climate Change 2013: The Physical Science Basis. Contribution of Working Group I to the Fifth Assessment Report of the Intergovernmental Panel On Climate Change. Cambridge University Press, Cambridge, United Kingdom and New York, NY, USA.

Jarvis, P.G., James, G.B., Landsberg, J.J., 1976. Coniferous forest, in: Vegetation and the Atmosphere. Academic Press, San Diego, California, USA, pp. 171–236.

Jiménez-Muñoz, J.C., Mattar, C., Barichivich, J., Santamaría-Artigas, A., Takahashi, K., Malhi, Y., Sobrino, J.A., van der Schrier, G., 2016. Record-breaking warming and extreme drought in the Amazon rainforest during the course of El Niño 2015–2016. Sci. Rep. 6, 33130. https://doi.org/10.1038/srep33130.

Kato, S., Loeb, N.G., Rose, F.G., Doelling, D.R., Rutan, D.A., Caldwell, T.E., Yu, L., Weller, R.A., 2012. Surface Irradiances Consistent with CERES-Derived Top-of-Atmosphere Shortwave and Longwave Irradiances. J. Clim. 26, 2719–2740. https://doi.org/10.1175/JCLI-D-12-00436.1.

Kim, W., Yeh, S.W., Kim, J.H., Kug, J.S., Kwon, M., 2011. The unique 2009–2010 El Niño event: A fast phase transition of warm pool El Niño to La Niña. Geophys. Res. Lett. 38, L15809. https://doi.org/10.1029/2011GL048521.

Koren, G., van Schaik, E., Araújo, A.C., Boersma, K.F., Gärtner, A., Killaars, L., Kooreman, M.L., Kruijt, B., van der Laan-Luijkx, I.T., von Randow, C., Smith, N.E., Peters, W., 2018. Widespread reduction in sun-induced fluorescence from the Amazon during the 2015/2016 El Niño. Philos. Trans. R. Soc. B Biol. Sci. 373, 20170408. https://doi.org/10.1098/rstb.2017.0408.

Koyama, K., Takemoto, S., 2014. Morning reduction of photosynthetic capacity before midday depression. Sci. Rep. 4, 4389. https://doi.org/10.1038/srep04389.

Longo, M., 2014. Amazon Forest Response to Changes in Rainfall Regime: Results from an Individual-Based Dynamic Vegetation Model.

Longo, M., Knox, R.G., Levine, N.M., Alves, L.F., Bonal, D., Camargo, P.B., Fitzjarrald, D. R., Hayek, M.N., Restrepo-Coupe, N., Saleska, S.R., Silva, R.da, Stark, S.C., Tapajós, R.P., Wiedemann, K.T., Zhang, K., Wofsy, S.C., Moorcroft, P.R., 2018. Ecosystem heterogeneity and diversity mitigate Amazon forest resilience to frequent extreme droughts. New. Phytol. 219, 914–931. https://doi.org/10.1111/nph.15185.

Mahadevan, P., Wofsy, S.C., Matross, D.M., Xiao, X., Dunn, A.L., Lin, J.C., Gerbig, C., Munger, J.W., Chow, V.Y., Gottlieb, E.W., 2008. A satellite-based biosphere parameterization for net ecosystem CO2 exchange: Vegetation Photosynthesis and Respiration Model (VPRM). Glob. Biogeochem. Cycles 22, B2005. https://doi.org/10.1029/2006GB002735.

Malhi, Y., Aragao, L.E.O.C., Metcalfe, D.B., Paiva, R., Quesadas, C.A., Almeida, S., Anderson, L., Brando, P., Chambers, J.Q., da Costa, A.C.L., Hutyra, L.R., Olivera, P., Patino, S., Pyle, E.H., Robertson, A.L., Texteira, L.M., 2009. Comprehensive assessment of carbon productivity, allocation and storage in three Amazonian forests. Glob. Change Biol. https://doi.org/10.1111/j.1365-2486.2008.01780.x.

Marengo, J.A., Espinoza, J.C., 2016. Extreme seasonal droughts and floods in Amazonia: causes, trends and impacts. Int. J. Climatol. 36, 1033–1050. https://doi.org/10.1002/joc.4420.

Masson-Delmotte, V., Zhai, P., Pörtner, H.O., Roberts, D., Skea, J., P.R.Shukla, Pirani, A., Moufouma-Okia, W., C.Péan, Pidcock, R., Connors, S., Matthews, J.B.R., Chen, Y., Zhou, X., Gomis, M.I., Lonnoy, E., Maycock, T., Tignor, M., (eds.), T.W., 2018. IPCC, 2018: Global warming of 1.5°C. AnIPCC Special Report on the impacts of global warming of 1.5°C above pre-industrial levels and related global greenhouse gas emission pathways, in the context of strengthening the global response to the threat of climate change, sustainable development, and efforts to eradicate poverty.

Meir, P., Metcalfe, D., Costa, A., Fisher, R., 2008. The fate of assimilated carbon during drought: impacts on respiration in Amazon rainforests. Philos. Trans. R. Soc. B Biol. Sci. 363, 1849–1855. https://doi.org/10.1098/rstb.2007.0021.

Miller, S.D., Goulden, M.L., Hutyra, L.R., Keller, M., Saleska, S.R., Wofsy, S.C., Figueira, A.M.S., Rocha, H.R.da, Camargo, P.B.de, 2011. Reduced impact logging minimally alters tropical rainforest carbon and energy exchange. Proc. Natl. Acad. Sci. U. S. A. 108, 19431. https://doi.org/10.1073/pnas.1105068108.

Monteith, J.L., 1972. Solar Radiation and Productivity in Tropical Ecosystem. J. Appl. Ecol. 9, 747–766. https://doi.org/10.2307/2401901.

Nepstad, D.C., Moutinho, P., Dias-Filho, M.B., Davidson, E., Cardinot, G., Markewitz, D., Figueiredo, R., Vianna, N., Chambers, J., Ray, D., Guerreiros, J.B., Lefebvre, P., Sternberg, L., Moreira, M., Barros, L., Ishida, F.Y., Tohlver, I., Belk, E., Kalif, K., Schwalbe, K., 2002. The effects of partial throughfall exclusion on canopy processes, aboveground production, and biogeochemistry of an Amazon forest. J. Geophys. Res. Atmospheres 107. https://doi.org/10.1029/2001JD000360. LBA 53-1-LBA 53-18.

Nepstad, D.C., Tohver, I.M., Ray, D., Moutinho, P., Cardinot, G., 2007. Mortality of Large Trees and Lianas Following Experimental Drought in an Amazon Forest. Ecology. 88, 2259–2269. https://doi.org/10.1890/06-1046.1.

Nobre, C.A., Sampaio, G., Borma, L.S., Castilla-Rubio, J.C., Silva, J.S., Cardoso, M., 2016. Land-use and climate change risks in the Amazon and the need of a novel sustainable development paradigm. Proc. Natl. Acad. Sci. 113, 10759–10768. https://doi.org/10.1073/pnas.1605516113.

Oke, T.R., 2015. Boundary Layer Climates. Routledge.

Oliveira de Morais, T.M., Berenguer, E., Barlow, J., França, F., Lennox, G.D., Malhi, Y., Chesini Rossi, L., Maria Moraes de Seixas, M., Ferreira, J., 2021. Leaf-litter production in human-modified Amazonian forests following the El Niño-mediated drought and fires of 2015–2016. For. Ecol. Manag. 496, 119441 https://doi.org/10.1016/j.foreco.2021.119441.

Phillips, O.L., Aragão, L.E.O.C., Lewis, S.L., Fisher, J.B., Lloyd, J., López-González, G., Malhi, Y., Monteagudo, A., Peacock, J., Quesada, C.A., Heijden, G.van der, Almeida, S., Amaral, I., Arroyo, L., Aymard, G., Baker, T.R., Bánki, O., Blanc, L., Bonal, D., Brando, P., Chave, J., Oliveira, Á.C.A.de, Cardozo, N.D., Czimczik, C.I., Feldpausch, T.R., Freitas, M.A., Gloor, E., Higuchi, N., Jiménez, E., Lloyd, G., Meir, P., Mendoza, C., Morel, A., Neill, D.A., Nepstad, D., Patiño, S., Peñuela, M.C., Prieto, A., Ramírez, F., Schwarz, M., Silva, J., Silveira, M., Thomas, A.S., Steege, H. ter, Stropp, J., Vásquez, R., Zelazowski, P., Dávila, E.A., Andelman, S., Andrade, A., Chao, K.J., Erwin, T., Fiore, A.D., C, E.H., Keeling, H., Killeen, T.J., Laurance, W.F., Cruz, A.P., Pitman, N.C.A., Vargas, P.N., Ramírez-Angulo, H., Rudas, A., Salamão, R., Silva, N., Terborgh, J., Torres-Lezama, A., 2009. Drought Sensitivity of the Amazon Rainforest. Science (1979) 323, 1344–1347. https://doi.org/10.1126/science.1164033.

Pyle, E.H., Santoni, G.W., Nascimento, H.E.M., Hutyra, L.R., Vieira, S., Curran, D.J., Haren, J., Saleska, S.R., Chow, V.Y., Carmago, P.B., Laurance, W.F., Wofsy, S.C., 2008. Dynamics of carbon, biomass, and structure in two Amazonian forests. J. Geophys. Res.Biogeosci. 113, 20. G00B08.

Restrepo-Coupe, N., da Rocha, H.R., da Araujo, A.C., Borma, L.S., Christoffersen, B., Cabral, O.M.R., de Camargo, P.B., Cardoso, F.L., da Costa, A.C.L., Fitzjarrald, D.R., Goulden, M.L., Kruijt, B., Maia, J.M.F., Malhi, Y.S., Manzi, A.O., Miller, S.D., Nobre, A.D., von Randow, C., Sá, L.D.A., Sakai, R.K., Tota, J., Wofsy, S.C., Zanchi, F. B., Saleska, S.R., 2013. What drives the seasonality of photosynthesis across the Amazon basin? A cross-site analysis of eddy flux tower measurements from the Brasil flux network. Agric. For. Meteorol. 182–183, 128–144.

Restrepo-Coupe, N., Levine, N.M., Christoffersen, B.O., Albert, L.P., Wu, J., Costa, M.H., Galbraith, D., Imbuzeiro, H., Martins, G., da Araujo, A.C., Malhi, Y.S., Zeng, X., Moorcroft, P., Saleska, S.R., 2017. Do dynamic global vegetation models capture the seasonality of carbon fluxes in the Amazon basin? A data-model intercomparison. Glob. Change Biol. 23, 191–208. https://doi.org/10.1111/gcb.13442.

Restrepo-Coupe, N., O'Donnell Christoffersen, B., Longo, M., Alves, L.F., Campos, K.S., da Araujo, A.C., de Oliveira Jr, R.C., Prohaska, N., da Silva, R., Tapajos, R., Wiedemann, K.T., Wofsy, S.C., Saleska, S.R., 2023. Asymmetric response of Amazon forest water and energy fluxes to wet and dry hydrological extremes reveals onset of a local drought-induced tipping point. Glob. Change Biol. 00 https://doi.org/10.1111/gcb.16933.

Rice, A.H., Pyle, E.H., Saleska, S.R., Hutyra, L.R., Palace, M., Keller, M., Camargo, P.B.de, Portilho, K., Marques, D.F., Wofsy, S.C., 2004. Carbon balance and vegetation dynamics in an old-growth Amazonian forest. Ecol. Appl. 14, S55–S71.

Ritchie, P.D.L., Parry, I., Clarke, J.J., Huntingford, C., Cox, P.M., 2022. Increases in the temperature seasonal cycle indicate long-term drying trends in Amazonia. Commun. Earth Environ. 3, 1–8. https://doi.org/10.1038/s43247-022-00528-0.

Saleska, S.R., Didan, K., Huete, A.R., da Rocha, H.R., 2007. Amazon Forests Green-Up During 2005 Drought. Science (1979) 318, 612. https://doi.org/10.1126/science.1146663.

Saleska, S.R., Miller, S.D., Matross, D.M., 2003. Carbon in Amazon forests: Unexpected seasonal fluxes and disturbance-induced losses. Science (1979) 302, 1554–1557.

Schaaf, C., Wang, Z., 2015. MCD43C1 MODIS/Terra+Aqua BRDF/AlbedoModel Parameters Daily L3 Global 0.05Deg CMG V006. [WWW Document]. In: Distrib. NASA EOSDIS Land Process. DAAC. https://doi.org/10.5067/MODIS/MCD43C1.006. URL(accessed 3.30.21).

Schaaf, C.B., Gao, F., Strahler, A.H., Lucht, W., Li, X., Tsang, T., Strugnell, N.C., Zhang, X., Jin, Y., Muller, J.P., Lewis, P., Barnsley, M., Hobson, P., Disney, M., Roberts, G., Dunderdale, M., Doll, C., d'Entremont, R.P., Hu, B., Liang, S., Privette, J.L., Roy, D., 2002. First operational BRDF, albedo nadir reflectance products from MODIS. Remote Sens. Environ., The Moderate Resolution Imaging Spectroradiometer (MODIS): a new generation of Land Surface Monitoring 83, 135–148. https://doi.org/10.1016/S0034-4257(02)00091-3.

Scranton, K., Amarasekare, P., 2017. Predicting phenological shifts in a changing climate. Proc. Natl. Acad. Sci. 114, 13212–13217. https://doi.org/10.1073/pnas.1711221114.

Silver, W.L., Neff, J., McGroddy, M., Veldkamp, E., Keller, M., Cosme, R., 2000. Effects of Soil Texture on Belowground Carbon and Nutrient Storage in a Lowland Amazonian Forest Ecosystem. Ecosystems 3, 193–209. https://doi.org/10.1007/s100210000019.

Sitch, S., Huntingford, C., Gedney, N., Levy, P.E., Lomas, M., Piao, S.L., Betts, R., Ciais, P., Cox, P., Friedlingstein, P., Jones, C.D., Prentice, I.C., Woodward, F.I., 2008. Evaluation of the terrestrial carbon cycle, future plant geography and climate-carbon cycle feedbacks using five Dynamic Global Vegetation Models (DGVMs). Glob. Change Biol. 14, 2015–2039. https://doi.org/10.1111/j.1365-2486.2008.01626.x.

Smith, M.N., Stark, S.C., Taylor, T.C., Ferreira, M.L., Oliveira, E.de, Restrepo-Coupe, N., Chen, S., Woodcock, T., Santos, D.B.dos, Alves, L.F., Figueira, M., Camargo, P.B.de, Oliveira, R.C.de, Aragão, L.E.O.C., Falk, D.A., McMahon, S.M., Huxman, T.E., Saleska, S.R., 2019. Seasonal and drought-related changes in leaf area profiles depend on height and light environment in an Amazon forest. New. Phytol. 222, 1284–1297. https://doi.org/10.1111/nph.15726.

Smith, M.N., Taylor, T.C., van Haren, J., Rosolem, R., Restrepo-Coupe, N., Adams, J., Wu, J., de Oliveira, R.C., da Silva, R., de Araujo, A.C., de Camargo, P.B., Huxman, T. E., Saleska, S.R., 2020. Empirical evidence for resilience of tropical forest photosynthesis in a warmer world. Nat. Plants 6, 1225–1230. https://doi.org/10.1038/s41477-020-00780-2.

Sombroek, W., 2001. Spatial and temporal patterns of Amazon rainfall. Consequences for the planning of agricultural occupation and the protection of primary forests. Ambio 30, 388–396.

Souza, M.L., Duarte, A.A., Lovato, M.B., Fagundes, M., Valladares, F., Lemos-Filho, J.P., 2018. Climatic factors shaping intraspecific leaf trait variation of a neotropical tree along a rainfall gradient. PLoS. One 13, e0208512. https://doi.org/10.1371/journal.pone.0208512.

Stoy, P.C., Katul, G.G., Siqueira, M.B.S., Juang, J.Y., Novick, K.A., Uebelherr, J.M., Oren, R., 2006. An evaluation of models for partitioning eddy covariance-measured net ecosystem exchange into photosynthesis and respiration. Agric. For. Meteorol. 141, 2–18. https://doi.org/10.1016/j.agrformet.2006.09.001.

Vieira, S., de Camargo, P.B., Selhorst, D., da Silva, R., Hutyra, L., Chambers, J.Q., Brown, I.F., Higuchi, N., dos Santos, J., Wofsy, S.C., Trumbore, S.E., Martinelli, L.A., 2004. Forest Structure and Carbon Dynamics in Amazonian Tropical Rain Forests. Oecologia 140, 468–479.

Wainwright, C.M., Allan, R.P., Black, E., 2022. Consistent Trends in Dry Spell Length in Recent Observations and Future Projections. Geophys. Res. Lett. 49, e2021GL097231.

Wehr, R., Saleska, S.R., 2021. Calculating canopy stomatal conductance from eddy covariance measurements, in light of the energy budget closure problem. Biogeosciences 18, 13–24. https://doi.org/10.5194/bg-18-13-2021.

Wu, J., Albert, L.P., Lopes, A.P., Restrepo-Coupe, N., Hayek, M., Wiedemann, K.T., Guan, K., Stark, S.C., Christoffersen, B., Prohaska, N., Tavares, J.V., Marostica, S., Kobayashi, H., Ferreira, M.L., Campos, K.S., Silva, R.da, Brando, P.M., Dye, D.G., Huxman, T.E., Huete, A.R., Nelson, B.W., Saleska, S.R., 2016. Leaf development and demography explain photosynthetic seasonality in Amazon evergreen forests. Science (1979) 351, 972–976. https://doi.org/10.1126/science.aad5068.

Wu, J., Guan, K., Hayek, M., Restrepo-Coupe, N., Wiedemann, K.T., Xu, X., Wehr, R., Christoffersen, B.O., Miao, G., da Silva, R., de Araujo, A.C., Oliviera, R.C., Camargo, P.B., Monson, R.K., Huete, A.R., Saleska, S.R., 2017. Partitioning controls on Amazon forest photosynthesis between environmental and biotic factors at hourly to interannual timescales. Glob. Change Biol. 23, 1240–1257. https://doi.org/10.1111/gcb.13509.

Xu, J., Lv, Y., Liu, X., Wei, Q., Qi, Z., Yang, S., Liao, L., 2019. A general non-rectangular hyperbola equation for photosynthetic light response curve of rice at various leaf ages. Sci. Rep. 9, 9909. https://doi.org/10.1038/s41598-019-46248-y.

Yang, H., Ciais, P., Wigneron, J.P., Chave, J., Cartus, O., Chen, X., Fan, L., Green, J.K., Huang, Y., Joetzjer, E., Kay, H., Makowski, D., Maignan, F., Santoro, M., Tao, S., Liu, L., Yao, Y., 2022. Climatic and biotic factors influencing regional declines and recovery of tropical forest biomass from the 2015/16 El Niño. Proc. Natl. Acad. Sci. 119, e2101388119 https://doi.org/10.1073/pnas.2101388119.

Zhang, K., de Almeida Castanho, A.D., Galbraith, D.R., Moghim, S., Levine, N.M., Bras, R. L., Coe, M.T., Costa, M.H., Malhi, Y., Longo, M., Knox, R.G., McKnight, S., Wang, J., Moorcroft, P.R., 2015. The fate of Amazonian ecosystems over the coming century arising from changes in climate, atmospheric CO2, and land use. Glob. Change Biol. 21, 2569–2587. https://doi.org/10.1111/gcb.12903.